International underground accelerator based lab for Nuclear Astrophysics

Dr. Cristina Bordeanu

HH-NIPNE

Romania

Physics of the Universe

Everywhere, our knowledge is incomplete and problems are waiting to be solved. We address the void in our knowledge and those unresolved problems by asking relevant questions and seeking answers to them.

Astrophysics

Observational astrophysics

Radio astronomy

Infrared astronomy

Optical astronomy

Ultraviolet, X-ray, gamma ray astronomy

gravitational wave

Neutrino

Cosmic rays

Theoretical astrophysics

analytical models
computational numerical simulations

stellar dynamics and evolution

galaxy formation

large-scale structure of matter in the Universe

origin of cosmic rays

general relativity and physical cosmology

string cosmology & astroparticle physics

Nuclear Astrophysics sites

Nuclear reaction rates at small energies needed in many **astrophysical models**

- -primordial nucleosynthesis,
- -stellar evolution,
- -novae,
- -supernovae, . . .

for **various processes**

- -pp chains,
- -CNO cycles,
- -s, r, p, rp, . . .

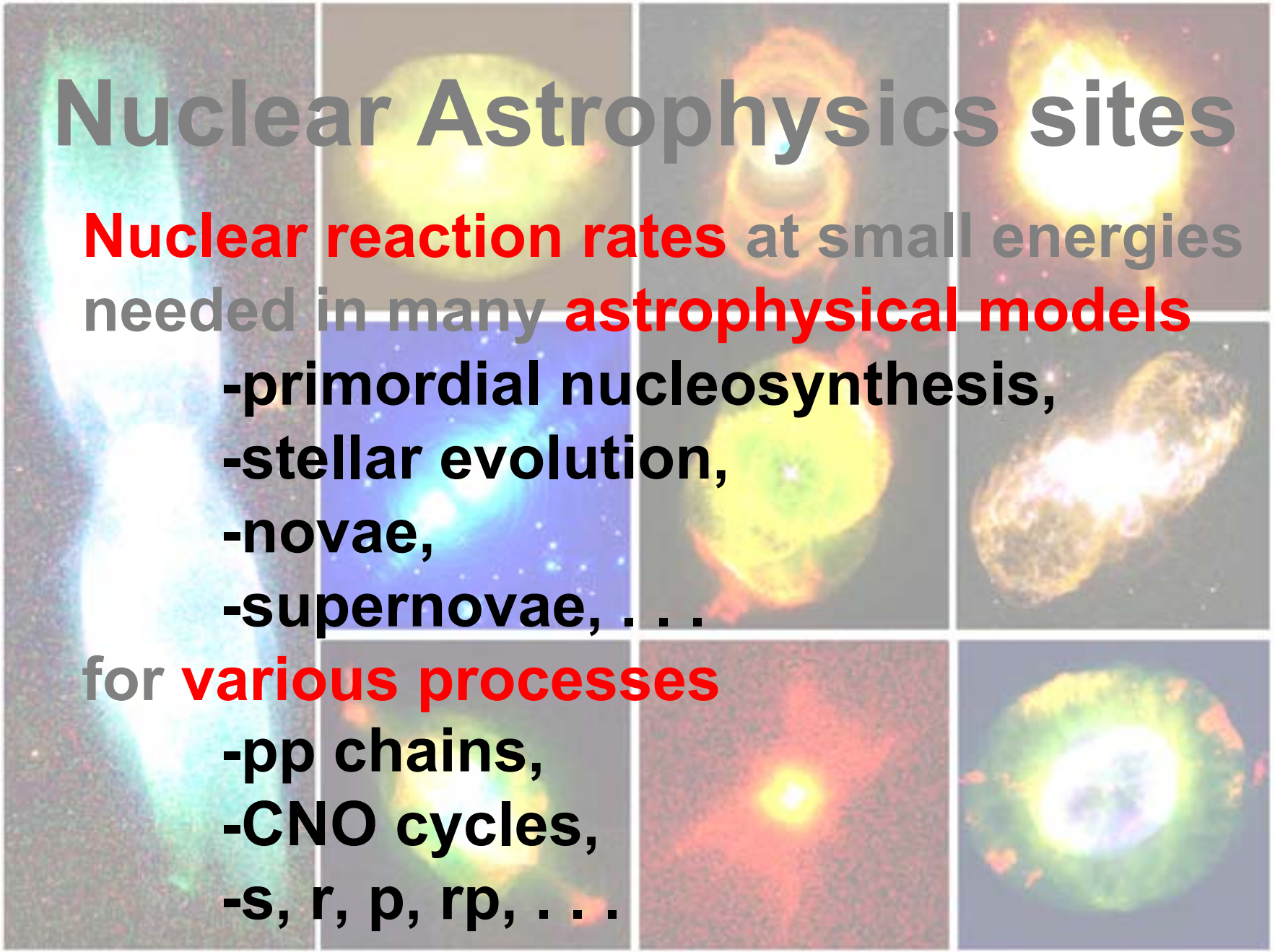

Unfortunately, there is no chance for us to study a star by placing our lab into a star!! Solutions?

- Accelerator based lab

1. On the ground level
2. Underground level
3. Into the ocean/sea water (not yet for an accelerator, but who knows – new Aquarium in the future …)

World underground labs:
-radioactive waste (most of them)
-physics labs (a few)
-seismic labs

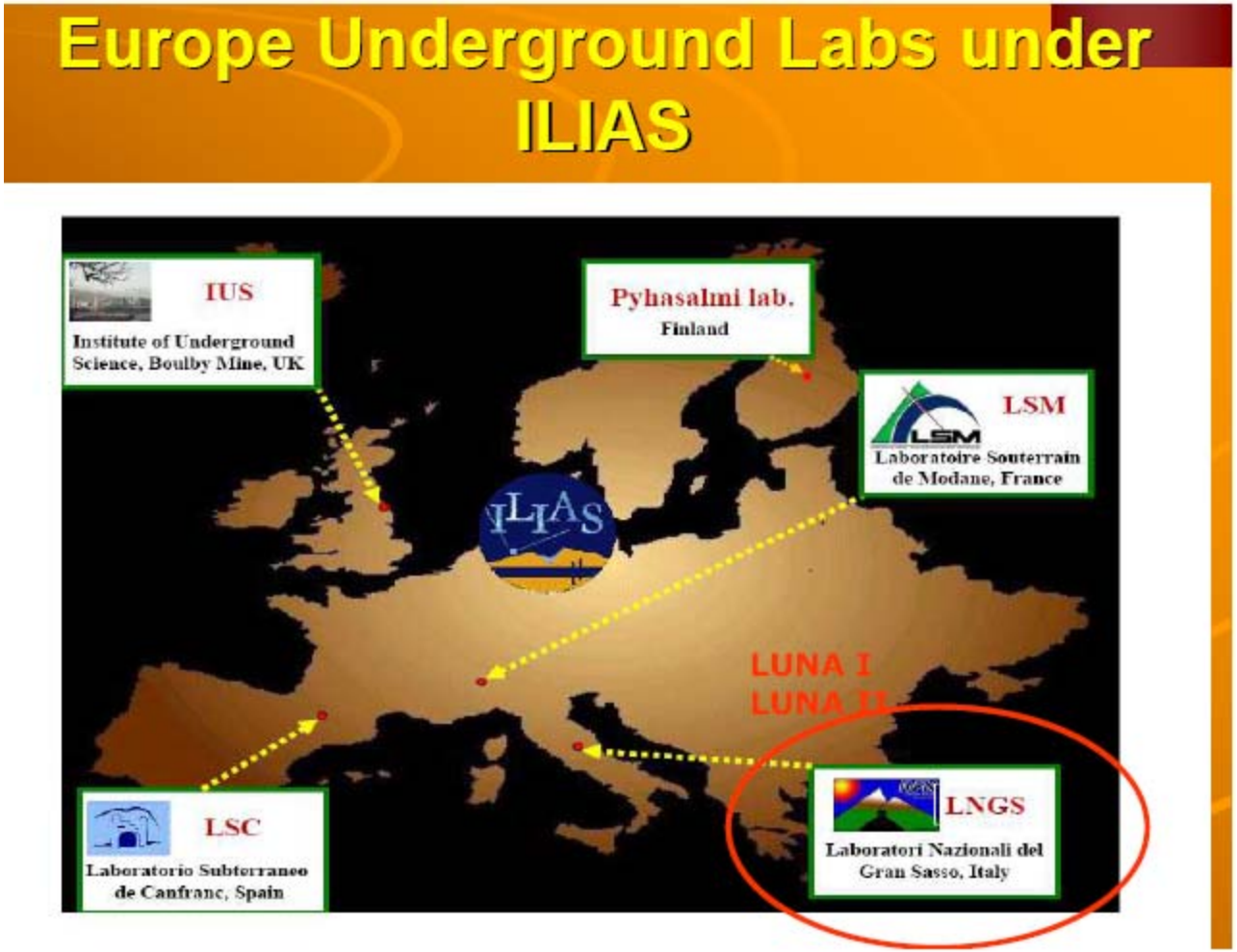

LUNA III (?)
Boulby (?)
Praid (?)

ECOS

"Many nuclear reactions across the periodic table play an important role in the aspects of nucleosynthesis.

However, there are about 20 reactions among light nuclides which play a decisive role in the energy production: hydrogen burning via the p-p chain and CNO cycles in main sequence stars and helium burning via $3\alpha \rightarrow {}^{12}C$, ${}^{12}C(\alpha,\gamma){}^{16}O$, ${}^{16}O(\alpha,\gamma){}^{20}Ne$ and ${}^{14}N(\alpha,\gamma){}^{18}F$ in red giants. These, helium burning reactions together with the ${}^{12}C+{}^{12}C$, ${}^{12}C+{}^{16}O$ and ${}^{16}O+{}^{16}O$ fusion reactions are also crucial for the evolution of a star of given mass and chemical composition, i.e. whether the star evolves into an early carbon-detonation supernova or into other supernovae of type I or type II. These H-, He- and C/O burning reactions are considered therefore as "key reactions" for nuclear astrophysics.

Clearly, they need to be known with fairly high precision if we want to understand the structure and evolution of stars and galaxies. These key reactions are extremely difficult to measure using the existing facilities and instrumentation."

+ NuPPEC

+ EURONS → ENSAR ….

Underground labs in USA

- Homestake gold mine 2600m deep (rock)
- WIPP New Mexico 700m deep (salt !! Quite a very different situation than rock)

Underground lab in Canada

- SNO (rock)

Underground Labs in Japan

facility	depth	Muon flux (/cm^2/sec)	Radon level	Neutron (cm^2/sec)	Experiment
Kamioka (Japan)	1000m	2×10^{-7}	20~60 Bq/m^3 (exp. Area)	8.3×10^{-6}	SK KamLAND
YangYang (Korea)	700m	4.4×10^{-7}	40~150 Bq/m^3	8×10^{-7}	KIMS
Oto cosmo (Japan)	467m	8×10^{-7}	~10 Bq/m^3	4×10^{-5}	ELEGANT
Ogoya (Japan)	135m	5×10^{-5}	~25 Bq/m^3	~2×10^{-5}	Ge detectors

Depth close to PRAID - Romania

6Bq / m^3 at PRAID - Romania

Reactions

- radiative capture/dissociation reactions
- with charged particles: (p;γ), (α;γ), . . .
- with neutrons: (n;γ), (γ;n)
- pure nuclear reactions: (p;α), (α;p), . . .
- weak interaction reactions: β^+, β^-, EC

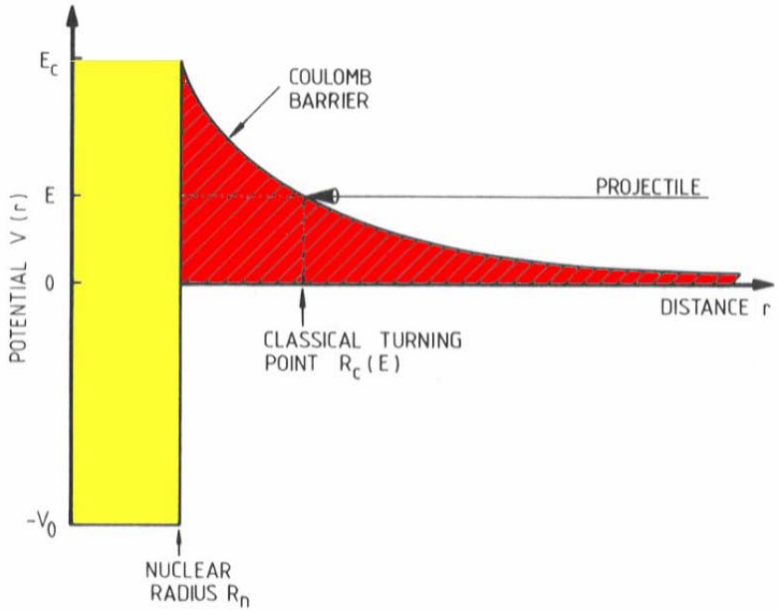

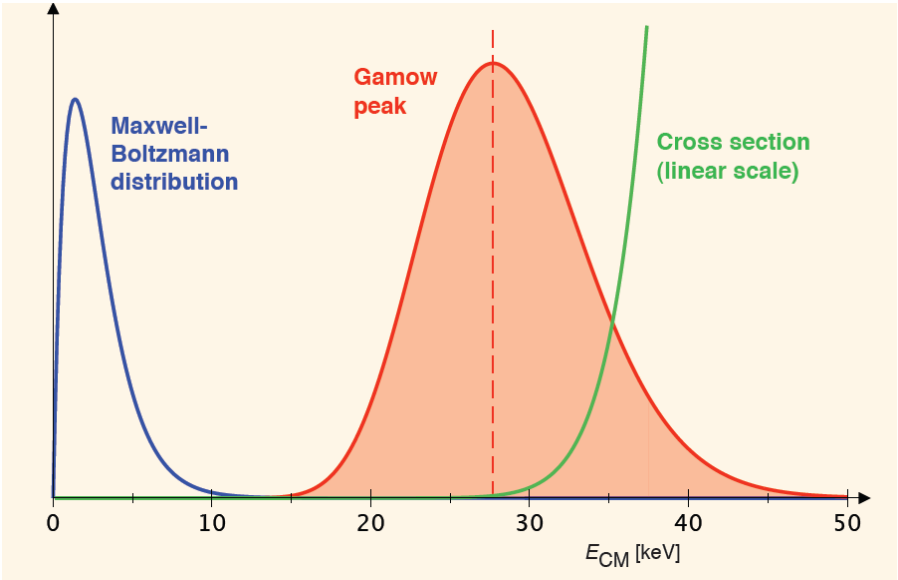

Measurements

- **direct measurements** preferable, but dificult: small energies/cross sections , often unstable nuclei involved
- **indirect methods** depending on type of reaction: charged-particle reactions → Coulomb dissociation, ANC method,Trojan-horse method
- What we chose? Depends on the accuracy required by the stellar model (1% or 30%).

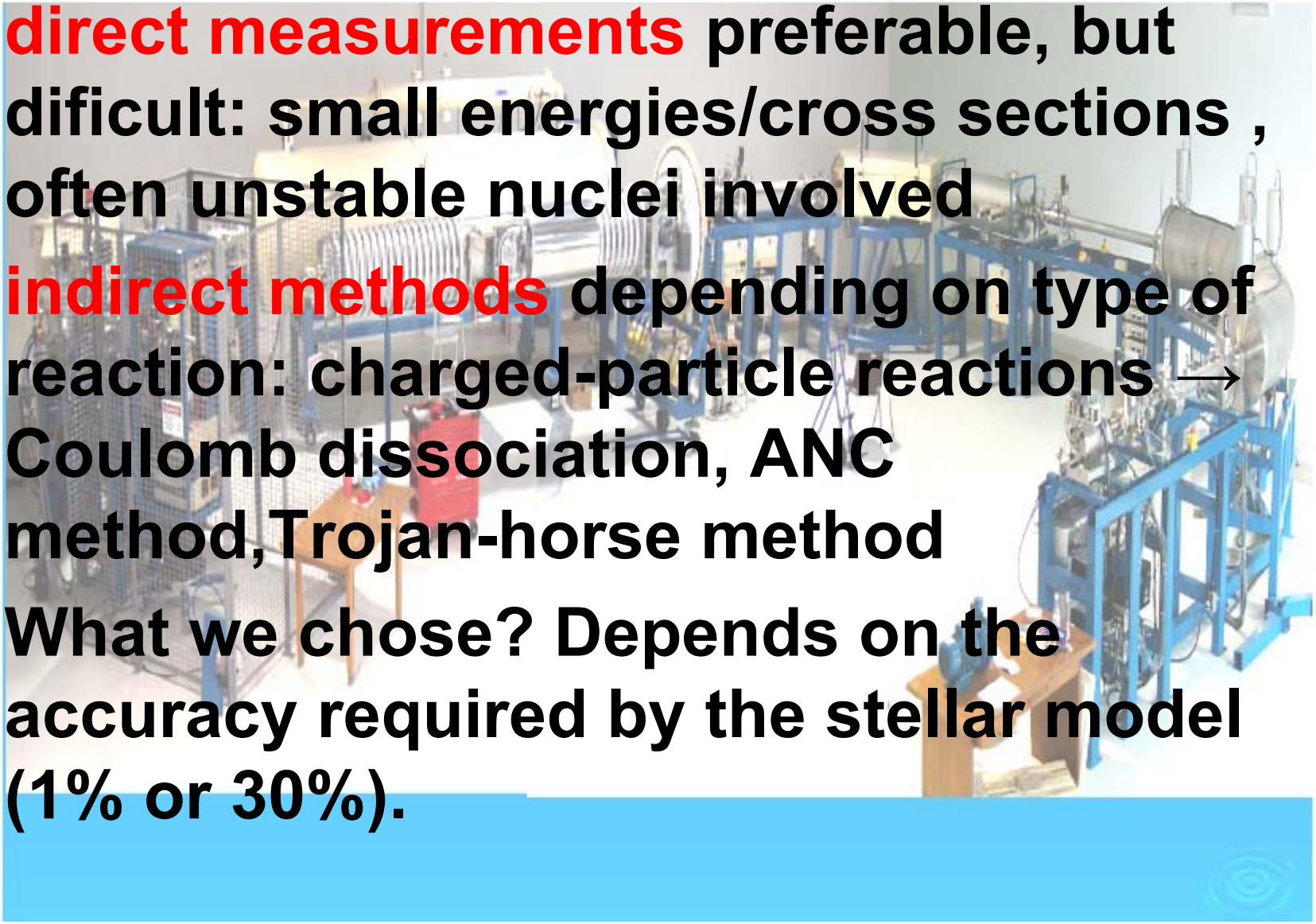

Nuclear Astrophysics with stable beams

- **Reactions with charged particles** → Coulomb barrier & strong energy dependence of cross sections. Cross sections are needed at small effective energy
- **Extrapolation** of measured cross sections to low energies with astrophysical S factor
- **Electron screening** in direct experiments → reduction of the Coulomb barrier & enhanced cross sections at low energies. Electron screening potential energy U_e presents a discrepancy between experimental observation and theoretical models

Stellar evolution

- **The role of individual reactions**
- **H-burning converts of ^{1}H into ^{4}He via pp-chains or the CNO-cycles. The simplest PPI chain is initiated by $^{1}H(p, e^{+}v)^{2}H(p,g)^{3}He$ and completed by $^{3}He(^{3}He,2p)^{4}He$. The dominant CNO-I cycle chain $^{12}C(p,g)^{13}N(e^{+}v)^{13}C(p,g)^{14}N(p,g)^{15}O(e^{+}v)^{15}N(p,a)^{12}C$ is controlled by the slowest reaction $^{14}N(p,g)^{15}O$.**
- **He-burning $^{4}He(2a,g)^{12}C$ (triple-alpha) and $^{12}C(a,g)^{16}O$**
- **C-burning $^{12}C(^{12}C, a)^{20}Ne$**
- **O-burning $^{16}O(^{16}O,a)^{28}Si$**

Background

1- Beam transport system
2- Reactions on target impurities
3- Elastic and inelastic beam scattering
4- Environmental radiation –
- detector activity
- room background
5- Cosmic rays

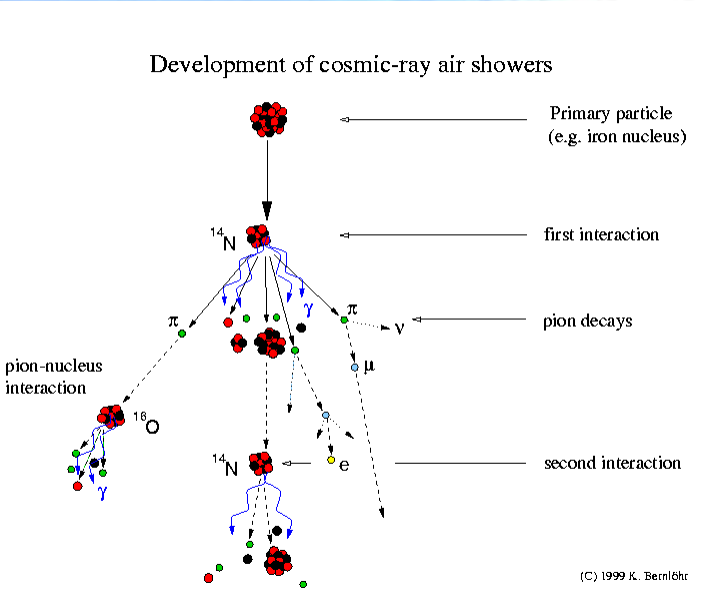

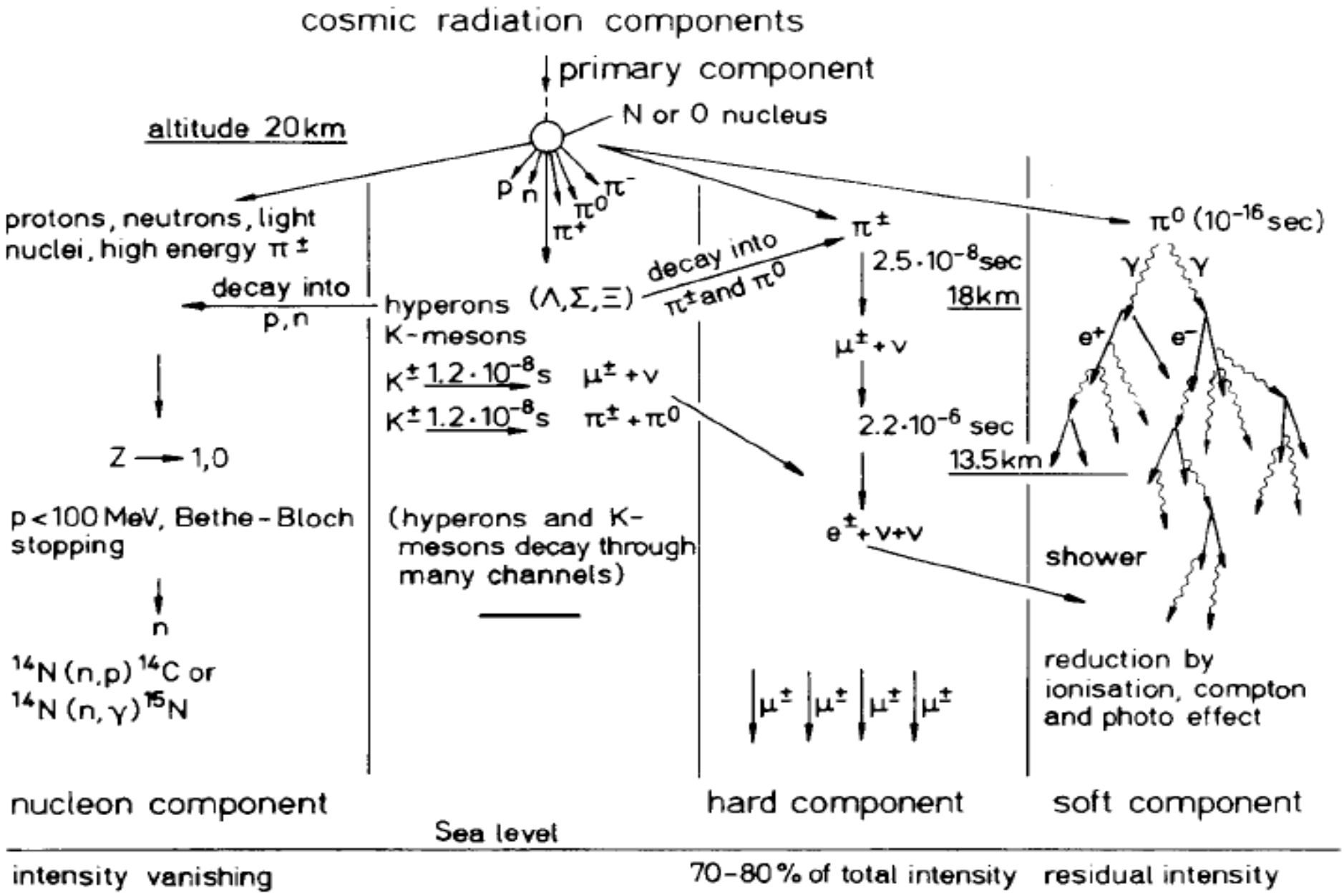

Fig. 1. Reaction scheme of cosmic rays with the atmosphere of the earth.

Laboratory background in gamma detectors underground

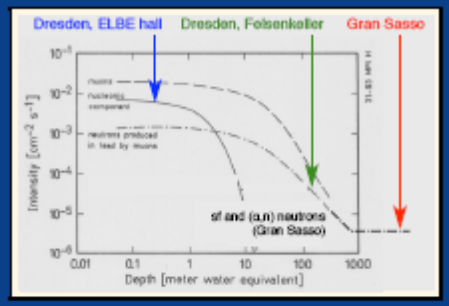

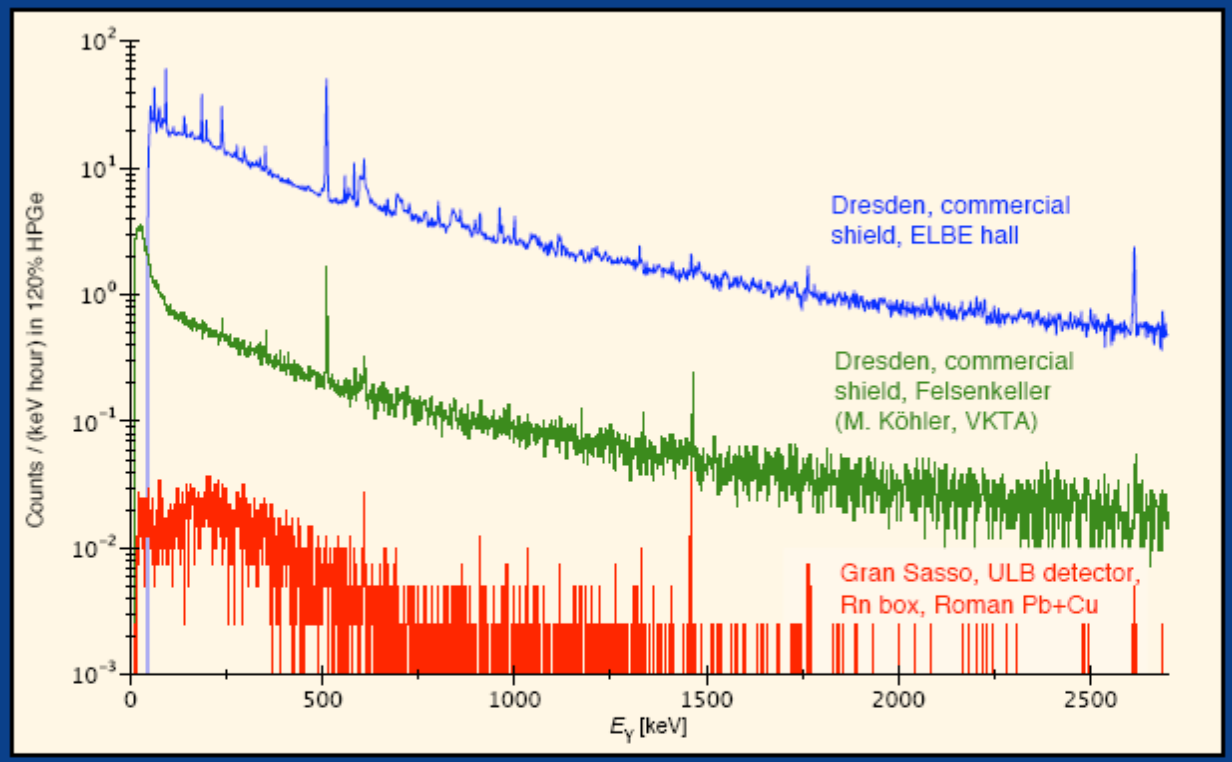

Muon flux
Neutron flux
Primordial radionuclides

3D Geometry

	LNGS	LSC	LSM	CUPP	Boulby	PRAID
Location	Motorway tunnel	Road tunnel	Road tunnel	Mine	Mine	Mine
Depth	1400 m	900 m	1750 m	1440 m	1100 m	120m
Access type	horizontal	horizontal	horizontal	vertical	vertical	Horizontal
Surface	13500 m2	1500 m2	500 m2		>1500 m2	>2200m2
Volume	180000 m3	10700 m3	3500 m3		3000 m3	>30000m3

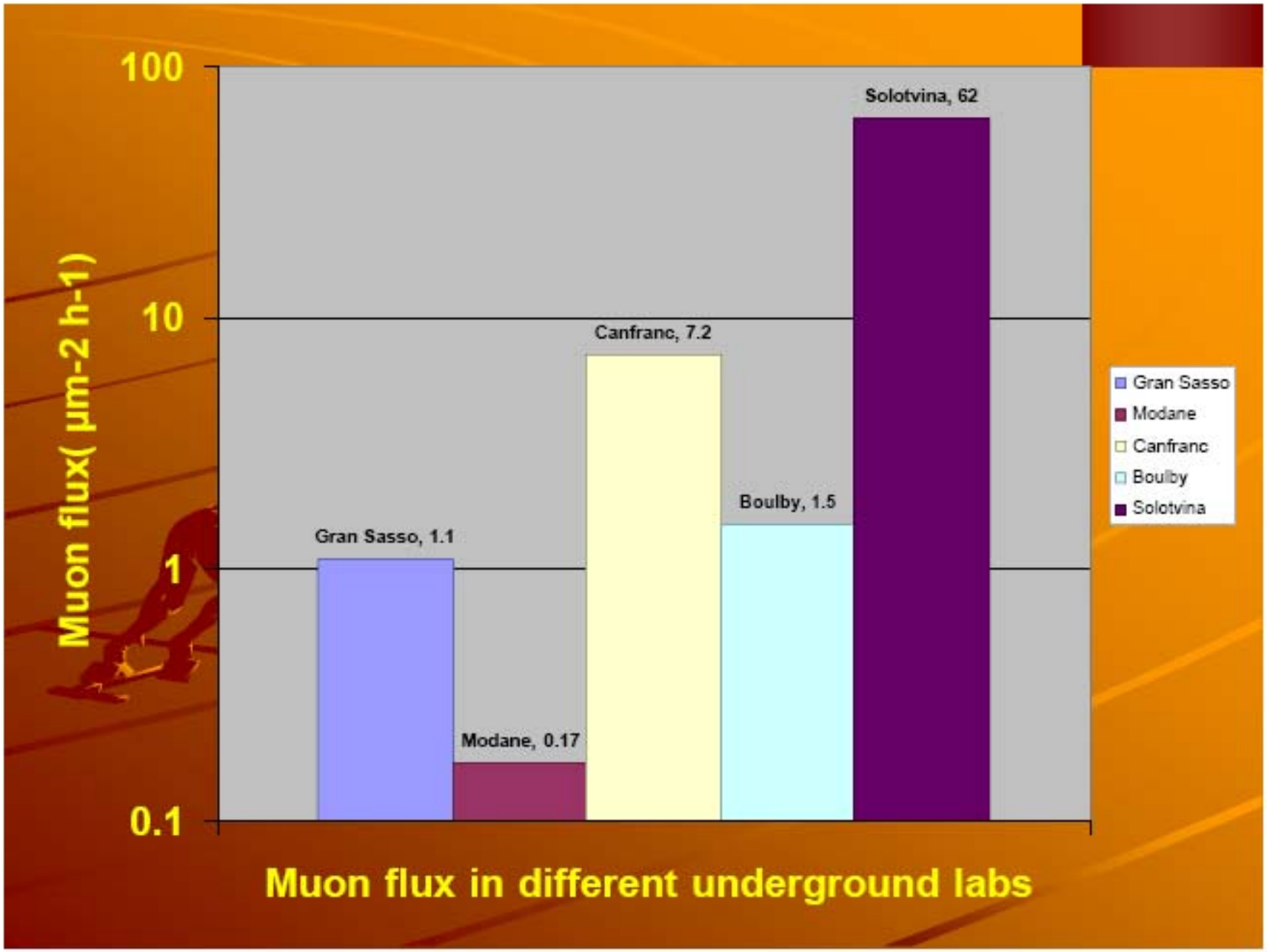
100
10
1
0.1
Muon flux(μm-2 h-1)
Gran Sasso, 1.1
Modane, 0.17
Canfranc, 7.2
Boulby, 1.5
Solotvina, 62
Gran Sasso
Modane
Canfranc
Boulby
Solotvina
Muon flux in different underground labs

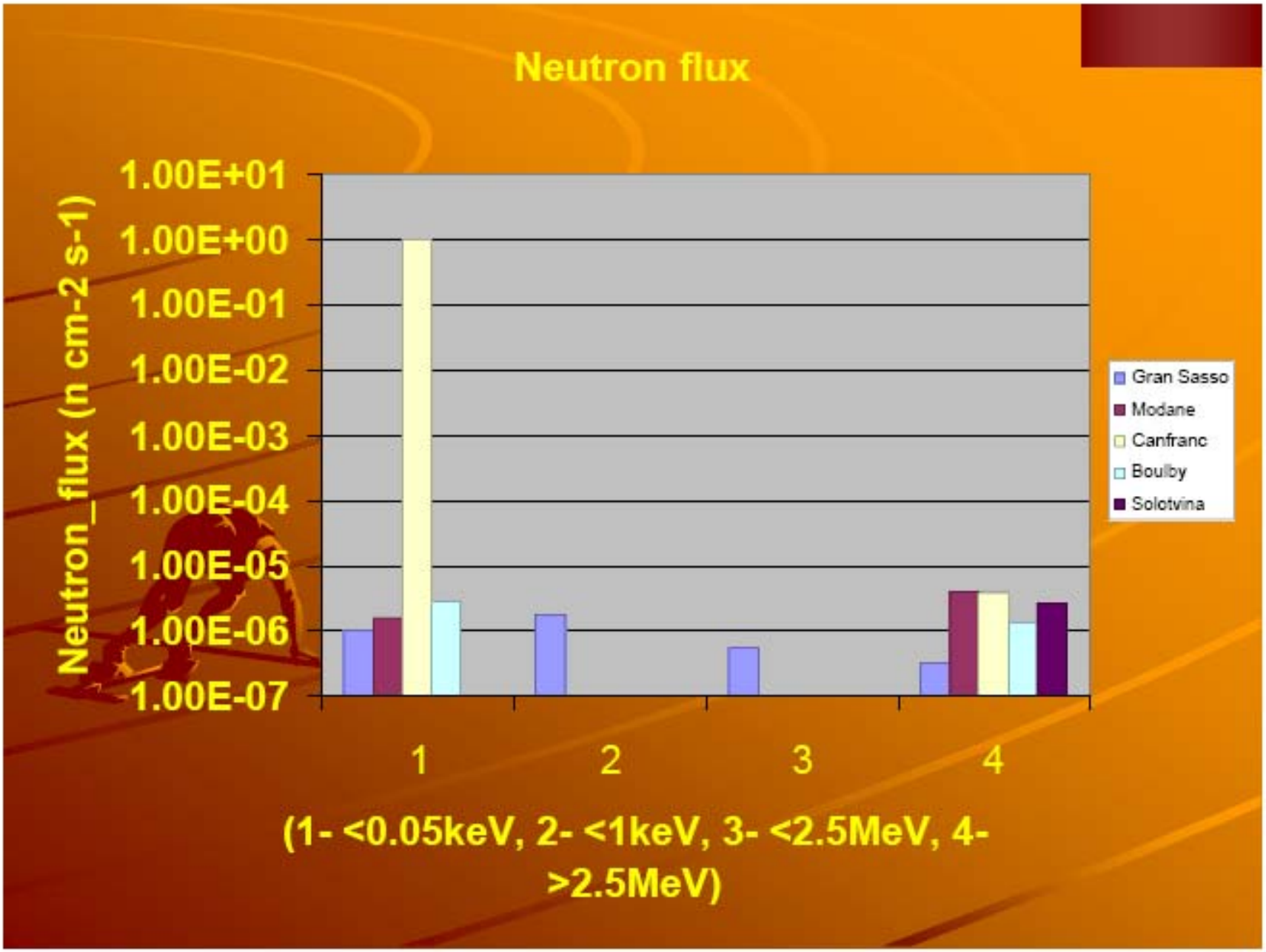
Neutron flux
Neutron_flux (n cm-2 s-1)
1.00E+01
1.00E+00
1.00E-01
1.00E-02
1.00E-03
1.00E-04
1.00E-05
1.00E-06
1.00E-07
1
2
3
4
(1- <0.05keV, 2- <1keV, 3- <2.5MeV, 4- >2.5MeV)
Gran Sasso
Modane
Canfranc
Boulby
Solotvina

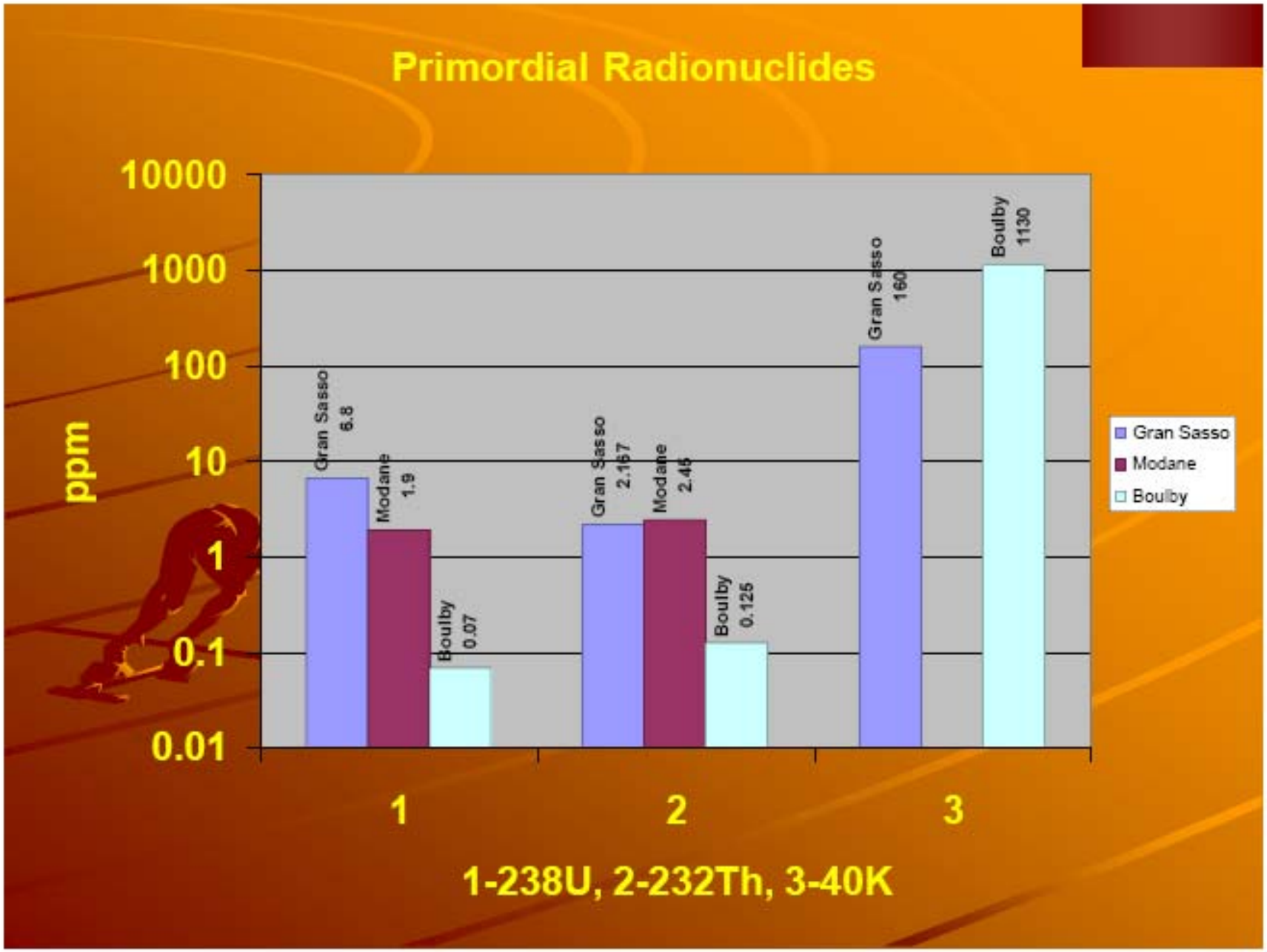
Primordial Radionuclides
10000
1000
100
10
1
0.1
0.01
ppm
Gran Sasso 6.8
Modane 1.9
Boulby 0.07
Gran Sasso 2.157
Modane 2.45
Boulby 0.125
Gran Sasso 160
Boulby 1130
Gran Sasso
Modane
Boulby
1
2
3
1-238U, 2-232Th, 3-40K

Uranium concentrations in our environment

Natural Uranium present in samples from ..	Average concentration of Uranium in samples ($\mu gU/cm^3$ or $\mu gU/g$) ($1\ \mu gU/cm^3$ or $1\ \mu gU/g = 1$ ppm U)	Radioactive concentration for the average concentration of Uranium in samples (Bq/cm^3 or Bq/g)	Remarks
Common rocks	0.5……4.7	6.67…..62.67	literature
Sol	1.9	25.33	literature
Ocean water	2.5×10^{-3}	33×10^{-3}	literature
Sea water	2.3×10^{-3}	31×10^{-3}	literature
Salt from sea water	6.3×10^{-3}	84×10^{-3}	calculation
Drink water	44×10^{-3}…….75×10^{-3}	59×10^{-2}…..100×10^{-2}	calculation
Human body (70 kg)	1.286×10^{-3}	17×10^{-6}	literature ($\mu gU/$ g body)
Salt samples (average)	10×10^{-3}	133×10^{-3}	Experiment for Slanic Prahova Salt

What is the proper way to measure contamination?

Boulby salt radiopurity

Material	Measured by	Method	^{238}U (ppb)	^{232}Th (ppb)	^{40}K (ppm)
Marine basalt(Fawcett)	Supplier's data	?	-	-	7000
Salt (Boulby cavern wall)	RAL	AA	-	-	> 400
Salt (Boulby cavern wall)	ICI Tracerco	NAA	< 60	< 100	-
Salt (Boulby cavern wall)	J.C. Barton	GES	10(10)	220(40)	750(50)
Salt (BSL, pure dried vacuum)	Supplier's data	?	-	-	< 240
Salt (ICI granulated)	RAL	AA	-	-	< 10
Salt (ICI, pure dried vacuum)	Supplier's data	?	-	-	15
Salt (ICI, pure dried vacuum)	RAL	AA	-	-	15
Salt (ICI, pure dried vacuum)	ICI Tracerco	NAA	5	30	-
Salt (ICI, pure dried vacuum)	Harwell (AEA Technology)(Harwell Scientifics after mid-1999)	ICPMS	< 6	30	-
Salt (WIPP cavern wall)	J.C. Barton	GES	440(80)	970(260)	4870(60)

DUSEL vs world

	Gran Sasso	Modane	DUSEL-	WIPP	Boulby	Praid
^{238}U (ppm)	6.8	1.9	0.08-0.16	0.06-0.44	0.07	0.01
^{232}Th (ppm)	2.167	2.45	0.25	0.03-0.97	0.125	
^{40}K (ppm)	160		1040	0.015-4.87	1130	
^{222}Rn (Bq/m^3)			37		10	6

LUNA Experiments

- **d+p › ^{3}He+γ E= 2.5keV Q: 5493.485 keV**
- **^{3}He+^{3}He › ^{4}He+2p E= 16.5keV Q: 11487.942 keV**
- **^{3}He+^{4}He › ^{7}Be+ γ E=100 keV Q: 1586.627 keV**
-
- **^{14}N+p › ^{15}O+ γ E= 70 keV Q: 7296.999 keV**
- **^{15}N+p › ^{16}O+ γ E= keV Q: 12127.406 keV**

Where are we now?

Low energy beams requires new ways to deal with them → ion source, accelerator, detectors, backgrounds

Nuclear astrophysics done at :

1- ground level lab (what kind of physics may be done here, needs for the acc. & detectors)

2- underground lab (what kind of physics deserves to be done there)

What experiments will be done at LUNA? Shall we repeat them? Which conditions?

What detectors are available? New detectors? Monte Carlo simulations

What ion sources are known now? New sources?

what else might be studied underground?

$^{12}C(\alpha,\gamma)$, $^{16}O(\alpha,\gamma)$ — *Supernovae ~ He burning*

$^{14}N(\alpha,\gamma)$
$^{18}O(\alpha,\gamma)$
$^{22}Ne(\alpha,\gamma)$
} *AGB stars ~ s process*

$^{14}N(p,\gamma)$
$^{17}O(p,\gamma)$
$^{17}O(p,\alpha)$
} *Red giants ~ CNO cycle*

$^{22}Ne(p,\gamma)$
$^{23}Na(p,\alpha)$
$^{24}Mg(p,\gamma)$
} *Globular clusters ~ Ne/Mg/Na cycles*

^{20}Ne, ^{24}Mg, ^{28}Si, ^{32}S, ^{36}Ar, $^{40}Ca(\alpha,\gamma)$ — *Supernova nucleosynthesis*

Courtesy of J.C. Blackmon, Physics Division, ORNL

Synthesis of Heavy Elements

At high tempreatures a larger number of nuclear reactions are activated

C-burning $T \sim 10^9$ K

$^{12}C(^{12}C,\alpha)^{20}Ne$
$^{12}C(^{12}C,p)^{23}Ne$

$^{12}C(p,\gamma)^{13}N(\beta^+)^{13}C(\alpha,n)^{16}O$ $\quad$ $^{12}C(n,\gamma)^{13}C(\alpha,n)^{16}O$
$^{23}Mg(n,\gamma)^{24}Mg(p,\gamma)^{25}Al$
$^{16}O(\alpha,\gamma)^{20}Ne$
$^{20}Ne(n,\gamma)^{21}Ne$

$^{16}O(\alpha,\gamma)^{20}Ne$
$^{12}C(^{12}C,\alpha)^{20}Ne$
$^{12}C(^{12}C,p)^{23}Na$ → $(p,\alpha)^{20}Ne$, $(p,\gamma)^{24}Mg$, $(\alpha,p)^{23}Mg$
$^{22}Ne(\alpha,n)^{25}Mg(p,\gamma)^{26}Al(\beta^+)^{26}Mg(p,\gamma)^{27}Al$
$^{22}Ne(p,\gamma)^{23}Na$
$^{20}Ne(n,\gamma)^{21}Ne(\alpha,n)^{24}Mg$
$^{20}Ne(\alpha,\gamma)^{24}Mg$
$^{12}C(n,\gamma)^{13}C(\alpha,n)^{16}O$

Ne-burning $T \sim 1.3 \cdot 10^9$ K

$^{20}Ne(\gamma,\alpha)^{16}O$

$^{20}Ne(\alpha,\gamma)$, $^{21}Ne(\alpha,n)$ → ^{24}Mg → (α,γ), $(n,\gamma)^{25}Mg(\alpha,n)$ → $^{28}Si(\alpha,\gamma)^{32}S$

^{23}Na → $(\alpha,p)^{26}Mg$, $(p,\alpha)^{23}Ne$
$(\alpha,p)^{26}Mg$ → $(\alpha,n)^{29}Si$, $(p,\gamma)^{27}Al$
$(p,\gamma)^{27}Al$ → $(\alpha,p)^{30}Si$, $(n,\gamma)^{28}Al(\beta^-)^{28}Si$

$^{22}Ne(\alpha,n)^{25}Mg$

$^{20}Ne(n,\gamma)^{21}Ne$

$^{28}Si(n,\gamma)^{29}Si(n,\gamma)^{30}Si$

$^{25}Mg(n,\gamma)^{26}Mg$

How much Passive and Active shielding helps for *detector* background rate reduction

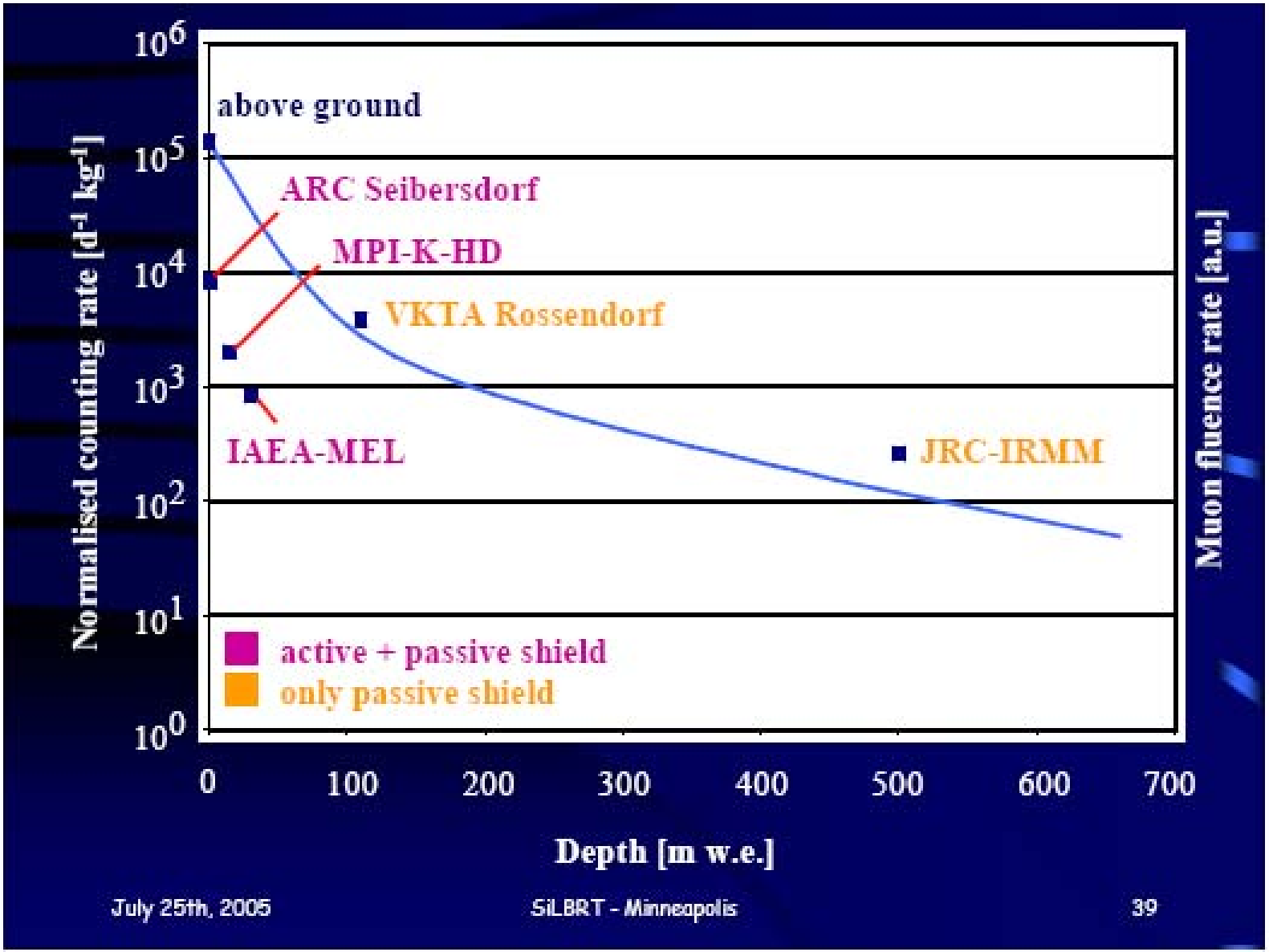

Lessons learned for the purity materials: detector shielding and detector materials

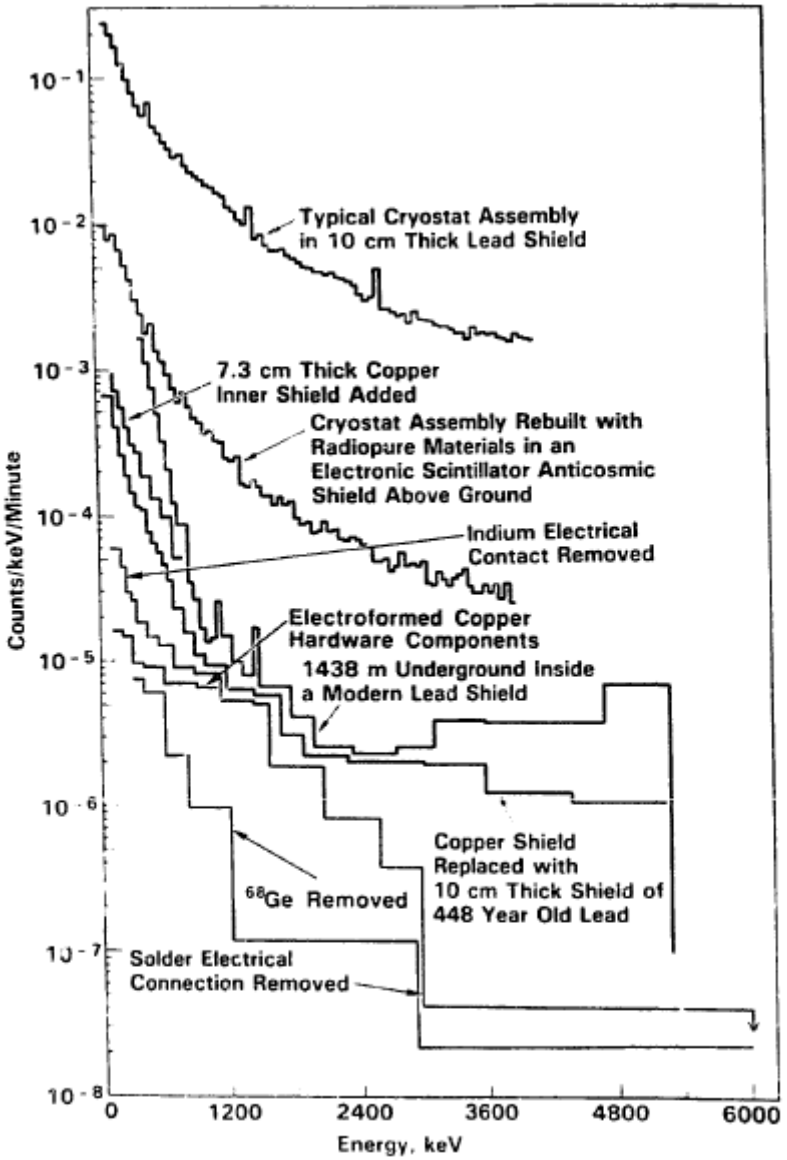

Fig. 1. Improvements in low-background technology.


Cacica
Praid
Slanic - Prahova
Chernovtsy
Suceava
Fălticeni
Paşcani
Iaşi
Piatra Neamţ
Bacău
Miercurea-Ciuc
Cluj-Napoca
Tirgu Mureş
Oradea
Satu Mare
Baia Mare
Sibiu
Braşov
Buzău
Ploieşti
Bucharest
Piteşti
Craiova
Constanţa
Galaţi
Brăila
Chişinau
Belgrade
Timişoara
Arad
Debrecen
Miskolc
TRANSYLVANIAN ALPS
Danube

Treatment base at Praid

Praid salt mine scheme

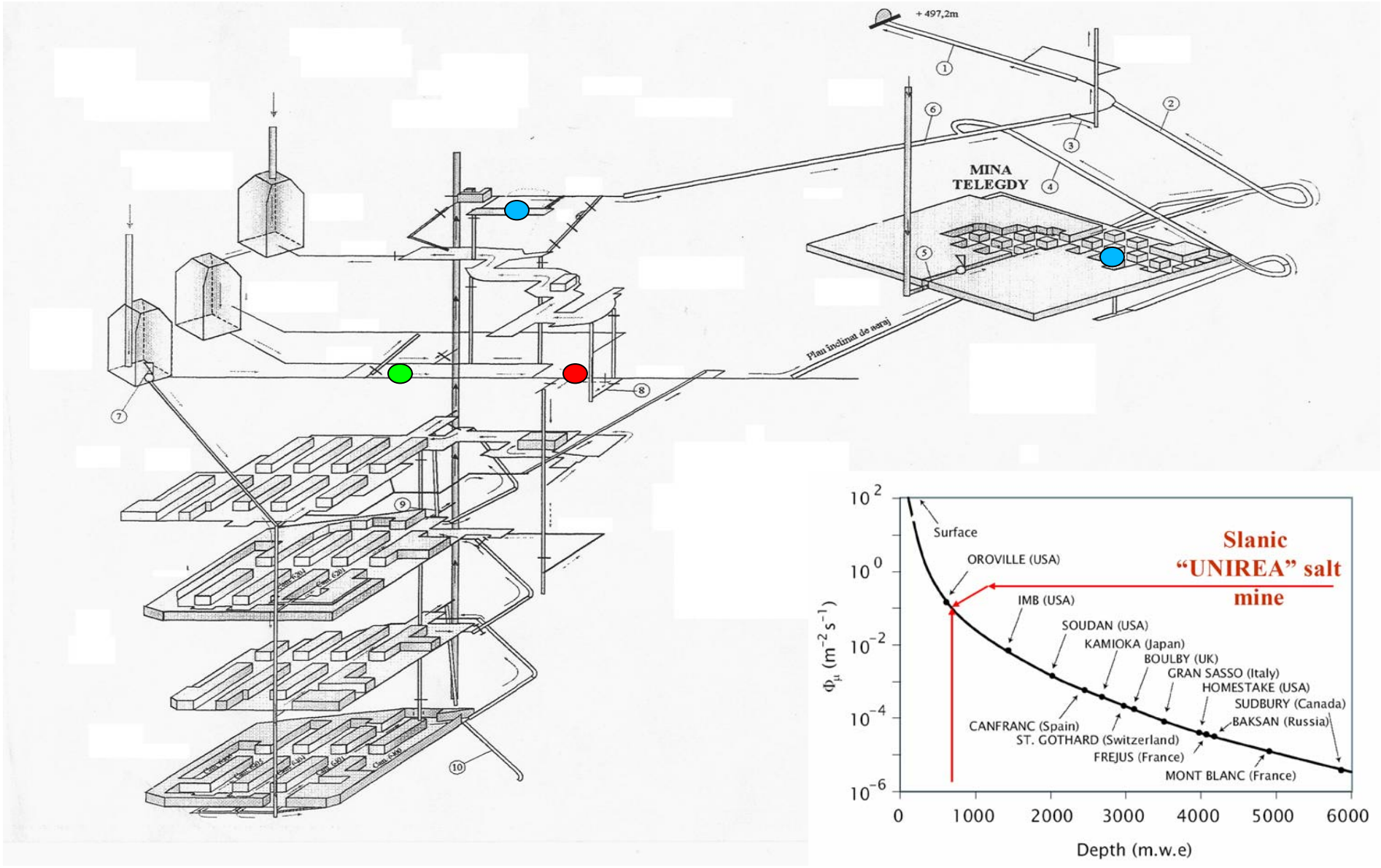

Praid characteristics

- High air purity
- Relative high air humidity: 71%
- condensed vapors: NaCl, Ca^{2+}, Mg, K, Na, I, Br,..
- High CO_2 concentration: 0.1-0.3%
- Negative air ionization: $^{222}Ra(1.5\text{-}1.9x10^{-13}Ci/l)$
- O^{3+} reduced concentration
- pH low: 6.5-6.9 (acid character)
- Oxygen partial pressure is bigger by 2.07%

Common elements found in the Earth's rocks.

Element	Chemical Symbol	Percent Weight in Earth's Crust
Oxygen	O	46.60
Silicon	Si	27.72
Aluminum	Al	8.13
Iron	Fe	5.00
Calcium	Ca	3.63
Sodium	Na	2.83
Potassium	K	2.59
Magnesium	Mg	2.09

Classification of some of the important minerals found in rocks.

Group	*Typical Minerals (and information link)*	*Chemistry*
Elements	Gold	Au
	Silver	Ag
	Copper	Cu
	Carbon (Diamond and Graphite)	C
	Sulfur	S
Sulfides	Cinnabar	HgS
	Galena	PBS
	Pyrite	FeS_2
Halides	Fluorite	CaF_2
	Halite	NaCl
Oxides	Corundum	Al_2O_3
	Cuprite	Cu_2O
	Hematite	Fe_2O_3
Carbonates (Nitrates and Borates)	Calcite	$CaCO_3$
	Dolomite	$CaMg(CO_3)_2$
	Malachite	$Cu_2(CO_3)(OH)_2$
Sulfates	Anhydrite	$CaSO_4$
	Gypsum	$CaSO_4 -2(H_2O)$
Phosphates (Arsenates, Vanadates, Tungstates, and Molybdates)	Apatite	$Ca_5(F,Cl,OH)(PO_4)$
Silicates	Albite	$NaAlSi_3O_8$
	Augite	(Ca, Na)(Mg, Fe, Al)(Al, Si)$_2O_6$
	Beryl	$Be_3Al_2(SiO_3)_6$
	Biotite	K (FE, Mg)$_3$$AlSi_3O_{10}(F, OH)_2$
	Hornblende	Ca_2(Mg, Fe, Al)$_5$(Al, Si)$_8O_{22}$(OH)$_2$
	Microcline	$KAlSi_3O_8$
	Muscovite	$KAl_2(AlSi_3O_{10})$(F, OH)$_2$
	Olivine	(Mg, Fe)$_2SiO_4$
	Orthoclase	$KAlSi_3O_8$
	Quartz	SiO_2
Organics	Amber	$C_{10}H_{16}O$

Salt radiochemistry Slanic Prahova

- Clor – ^{35}Cl, ^{37}Cl = 100%; no radioactive isotopes in the salt mine deposit
- Sulfur– ^{32}S, ^{33}S, ^{34}S, ^{36}S = 100%; no radioactive isotopes in the salt mine deposit
- Oxygen – ^{16}O, ^{17}O, ^{18}O = 100%; no radioactive isotopes in the salt mine deposit
- Sodium – ^{23}Na = 100%; no radioactive isotopes in the salt mine deposit
- Magnezium – ^{24}Mg, ^{25}Mg, ^{26}Mg = 100%; no radioactive isotopes in the salt mine deposit
- Aluminium – ^{27}Al = 100%; no radioactive isotopes in the salt mine deposit
- Potasium – ^{39}K, ^{41}K = 99.9883%; has 0.0117% radioactive isotopes into the salt mine deposit
- Calcium – ^{40}Ca, ^{42}Ca, ^{43}Ca, ^{44}Ca, ^{46}Ca = 99.81%; has 0.19% radioactive isotopes into the salt mine deposit
- Lead – ^{204}Pb, ^{206}Pb, ^{207}Pb, ^{208}Pb = 100%.

Slanic Prahova salt composition characterization by activation

Element	Atomic number	Concentration (ppb)
Na	24	$2.78*10^{+05}$
Al	28	$1.47*10^{+02}$
Cl	38	$6.29*10^{+05}$
Ca	49	$2.19*10^{+04}$
Ti	51	$2.26*10^{+03}$
V	52	$1.49*10^{+01}$
Mn	56	$6.17*10^{+01}$
Fe	59	$3.26*10^{+02}$
Co	60	$4.58*10^{-02}$
Cu	66	$7.97*10^{+02}$
Br	82	$1.26*10^{+00}$
U	239	$9.32*10^{-01}$

Gamma spectroscopy results

zone	Whole spectrum		time	2620-3000 keV	
	rate(cts/sec)	err(cts/sec)	(sec)	rate(cts/sec)	err(cts/sec)
Praid mine, orizont 60, detector in the center of the hall	*10.9916*	*0.0663*	*2501*	*0.0188*	*0.0027*
Praid mine, orizont 60, partial salt bricks shield	*4.9316*	*0.0248*	*8000*	*0.0053*	*0.0008*
Praid mine, orizont 60, detector close to the right wall	6.4643	0.0302	7109	0.0058	0.0009
Praid mine, orizont 60, detector close to left wall	8.1064	0.0403	5000	0.0016	0.0006
Praid mine, orizont 60, detector close to back left wall	13.5743	0.0583	4000	0.0030	0.0009
Praid mine, Telegdy, detector in the right center hall	23.9753	0.1264	1500	0.0133	0.0030
Praid mine, Doja mine, corridor near elevator	12.3000		240180	0.0006	0.0001
ground level (Sovata-Praid)	113.2504	0.1065	9989	0.0449	0.0021

Consistent results from TL dosimetry

Detectors type: GR200A

Exposure time: 107 days (102 inside mine)

Telegdy Hall: 3.86 +/- 0.23 nSv/h

“Orizont 60” Hall: 2.76 +/- 0.17 nSv/h

Ground level: 55.1 +/- 0.7 nSv/h

IFIN-HH Bucharest: 73.3 nSv/h

Background spectra at Praid w/wo Pb shielding

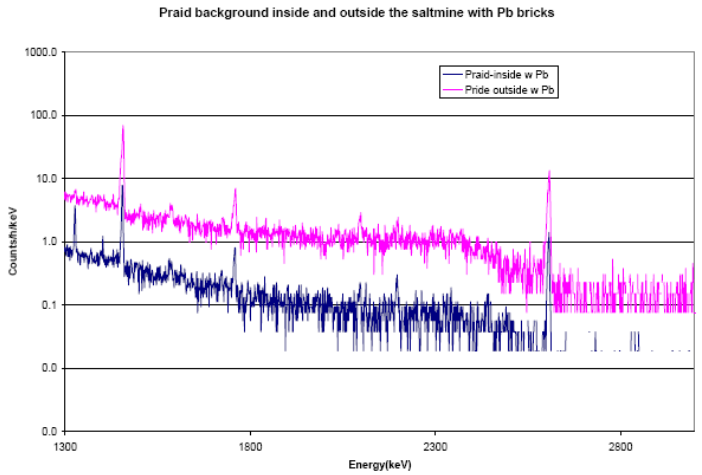

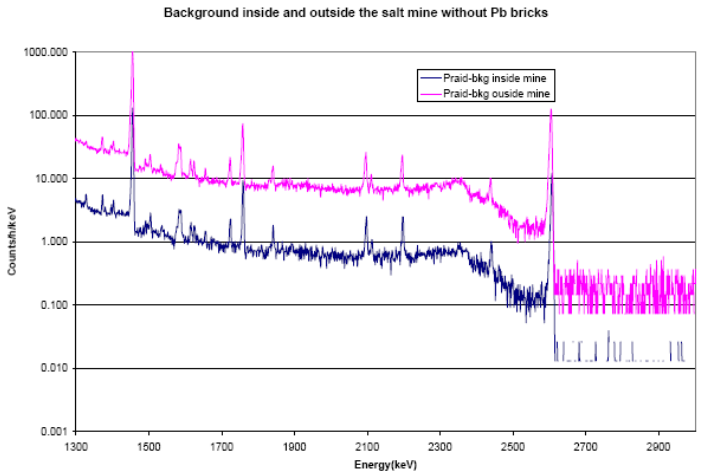

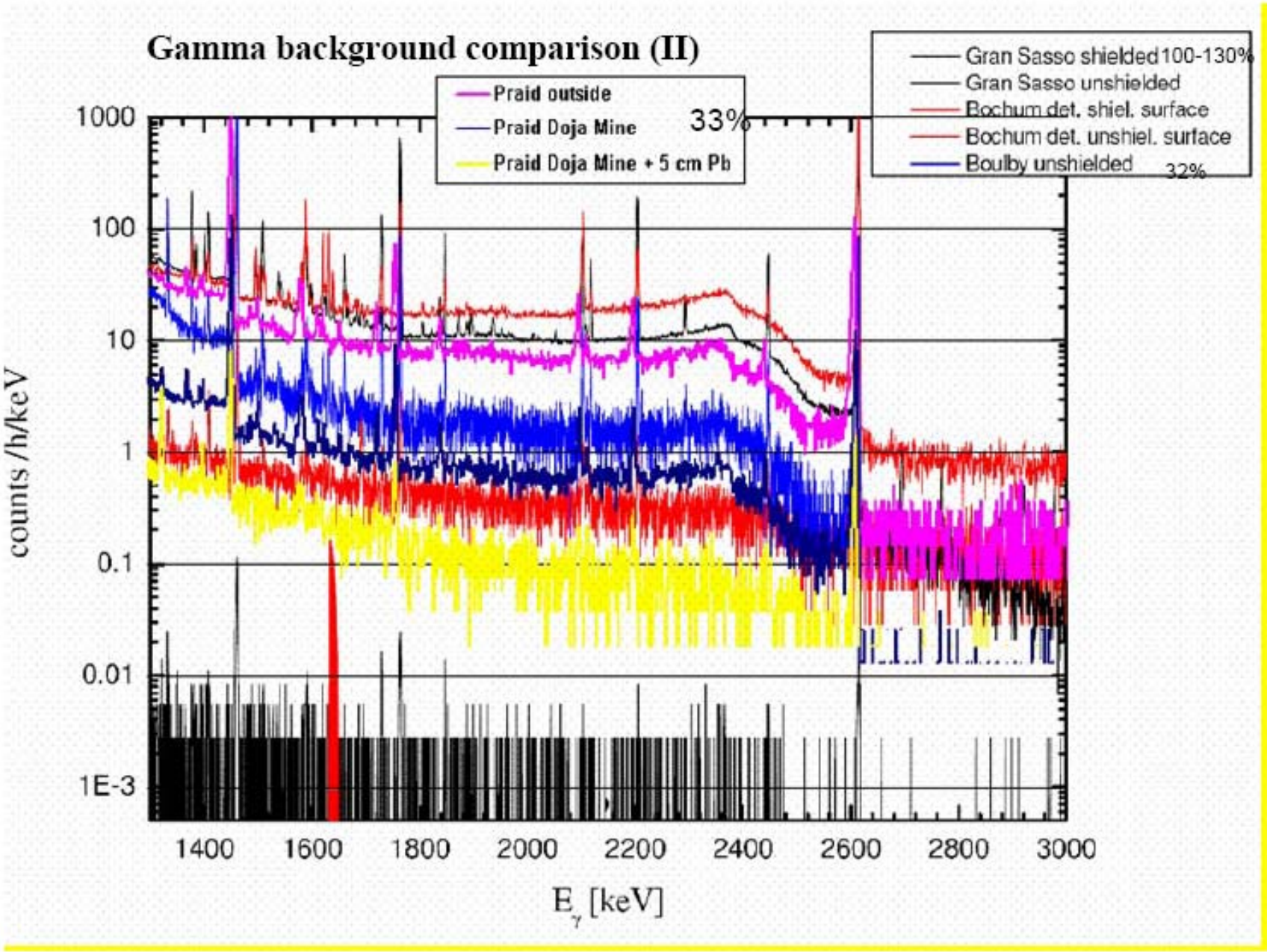
Gamma background comparison (II)
Praid outside
Praid Doja Mine
Praid Doja Mine + 5 cm Pb
33%
Gran Sasso shielded 100-130%
Gran Sasso unshielded
Bochum det. shiel. surface
Bochum det. unshiel. surface
Boulby unshielded
32%
counts /h/keV
1000
100
10
1
0.1
0.01
1E-3
1400
1600
1800
2000
2200
2400
2600
2800
3000
E_γ [keV]

Background spectra collected with an ORTEC GeHP detector with 33% rel. efficiency

Slanic Prahova salt mine

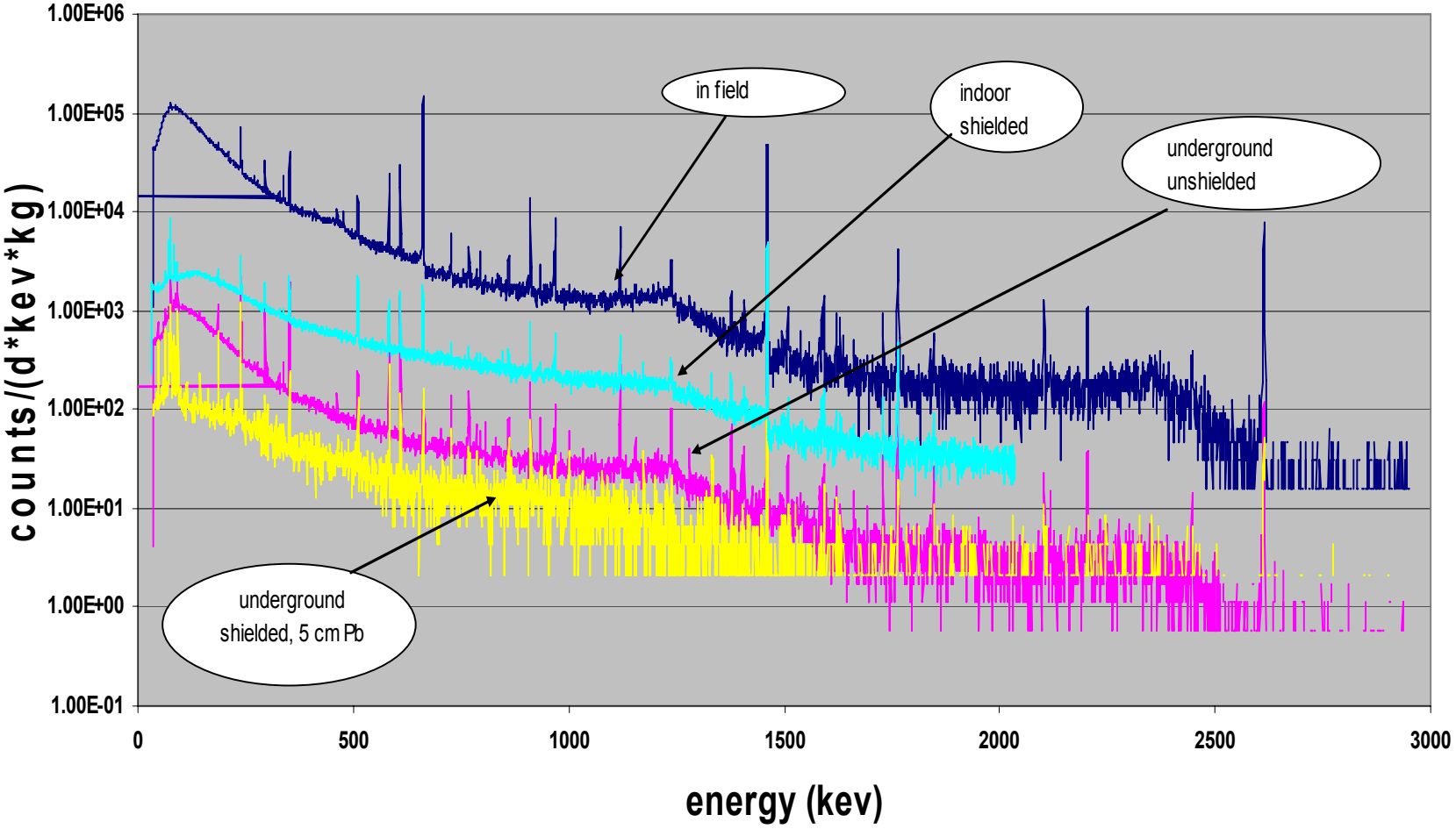


Elemental Formation in Stars
The Big Bang
Planetary System Formation
Forming Earth-like Planet
Chemistry of Life

$^3He+^4He \rightarrow \gamma+^7Be$ Weizmann 2004 & LUNA 2007

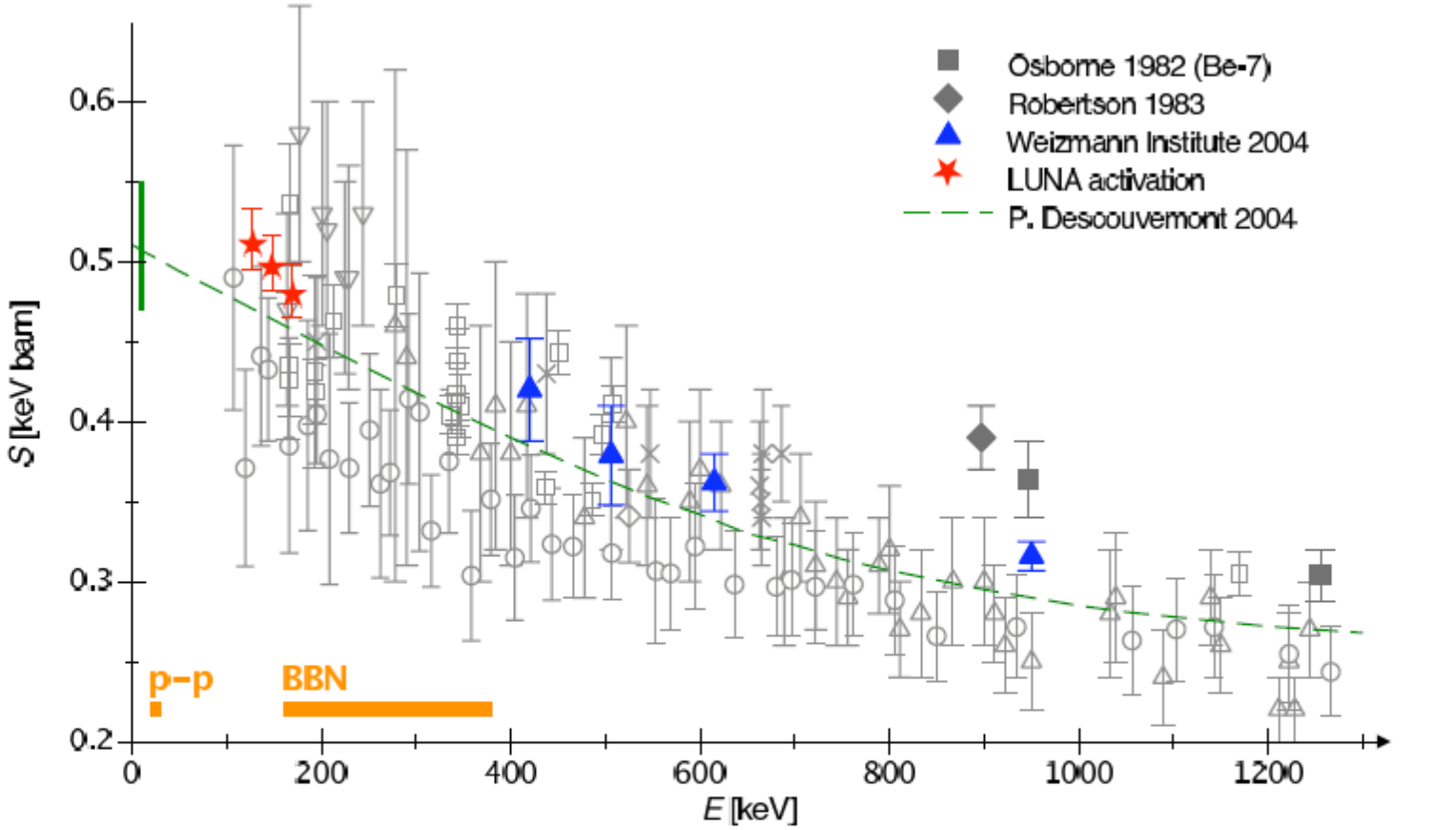

Figure 5. Astrophysical S-factor for $^3He(\alpha,\gamma)^7Be$. Activation data: filled squares [24], filled diamonds [25], filled triangles [21], stars (present work). Prompt-γ data: triangles [27], inverted triangles [28], circles [29] (renormalized by a factor 1.4 [20]), squares [24], diamonds [30], crosses [20]. Dashed line: previously adopted R-matrix fit [23]. Horizontal bars: energies relevant for p–p chain and for BBN.

Seattle 2007 $^{3}He+^{4}He \rightarrow \gamma+^{7}Be$

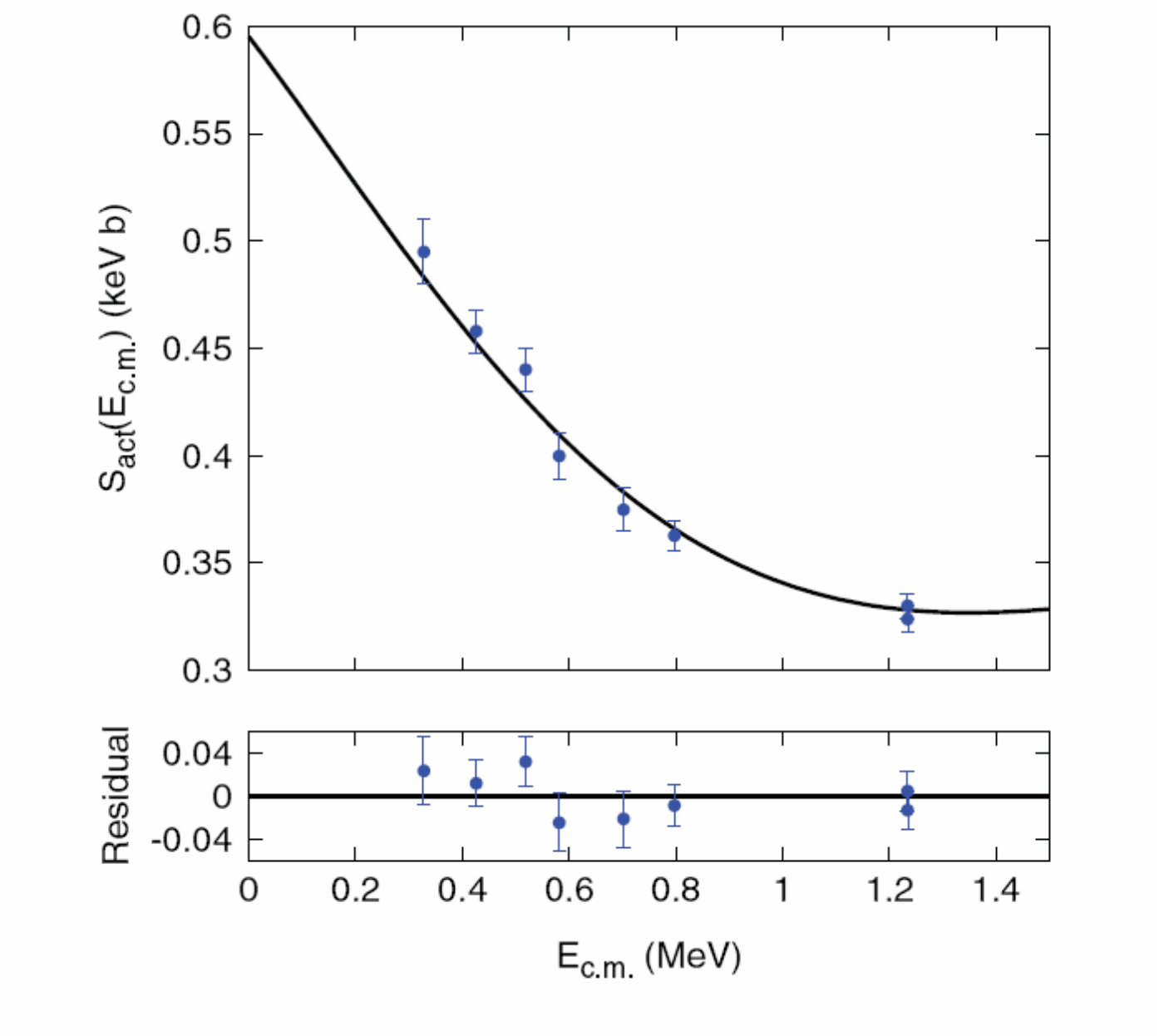

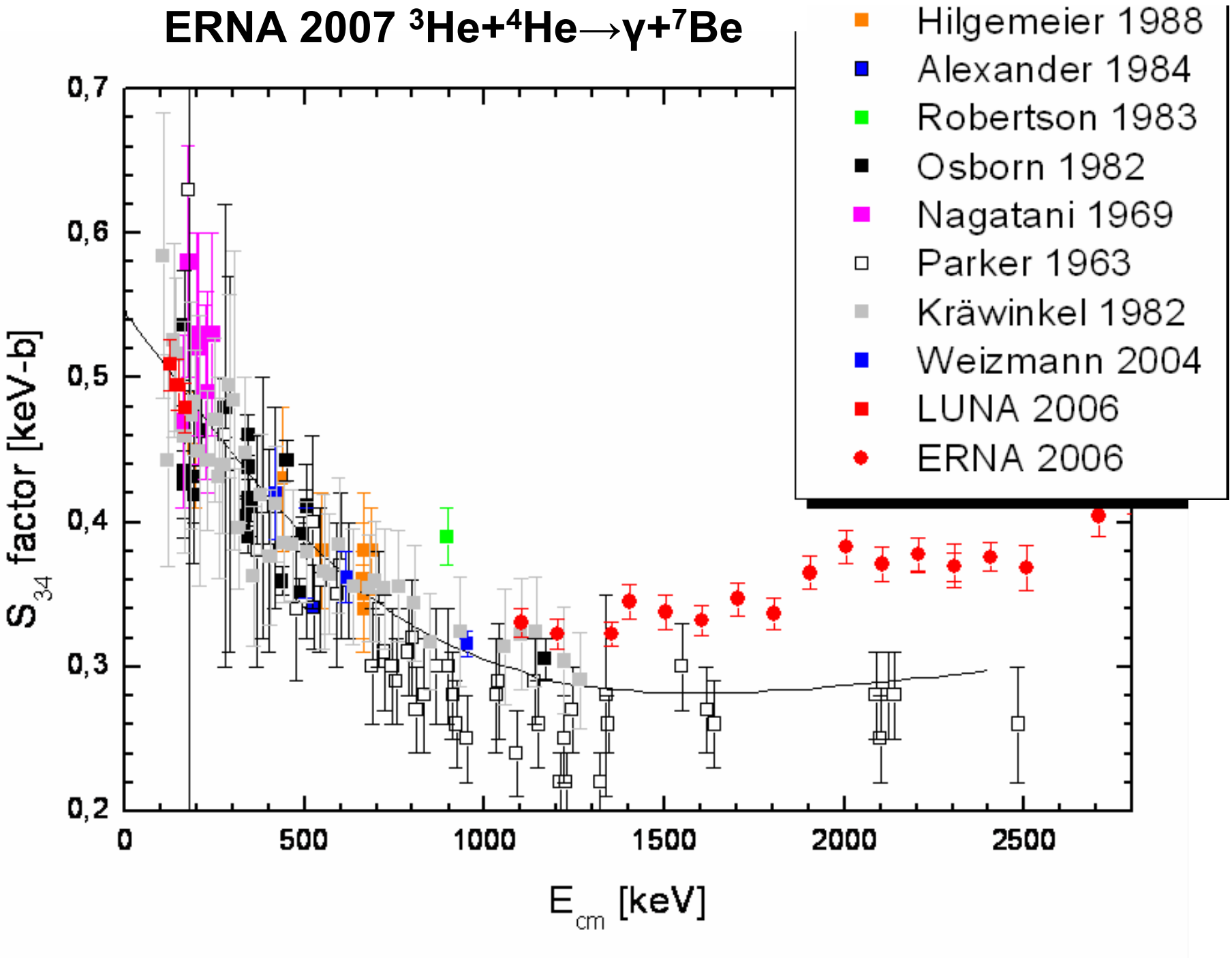
ERNA 2007 $^{3}He+^{4}He \rightarrow \gamma+^{7}Be$
Hilgemeier 1988
Alexander 1984
Robertson 1983
Osborn 1982
Nagatani 1969
Parker 1963
Kräwinkel 1982
Weizmann 2004
LUNA 2006
ERNA 2006
S_{34} factor [keV-b]
0,7
0,6
0,5
0,4
0,3
0,2
0
500
1000
1500
2000
2500
E_{cm} [keV]

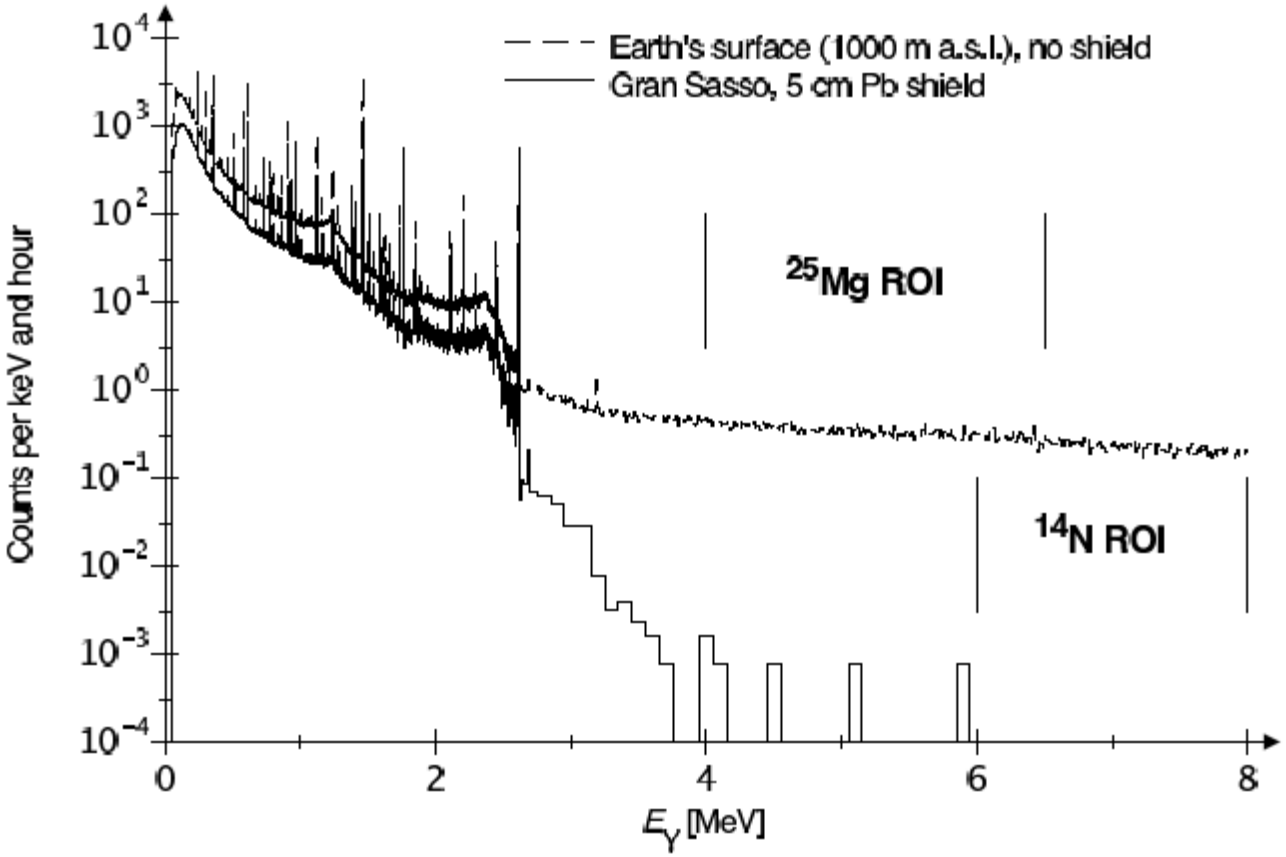

Fig. 2. Laboratory γ background as seen with the germanium detector of setup A at the earth's surface (1000 m above sea level) and inside the Gran Sasso underground facility.

d(p,γ)^{3}He LUNA 2002

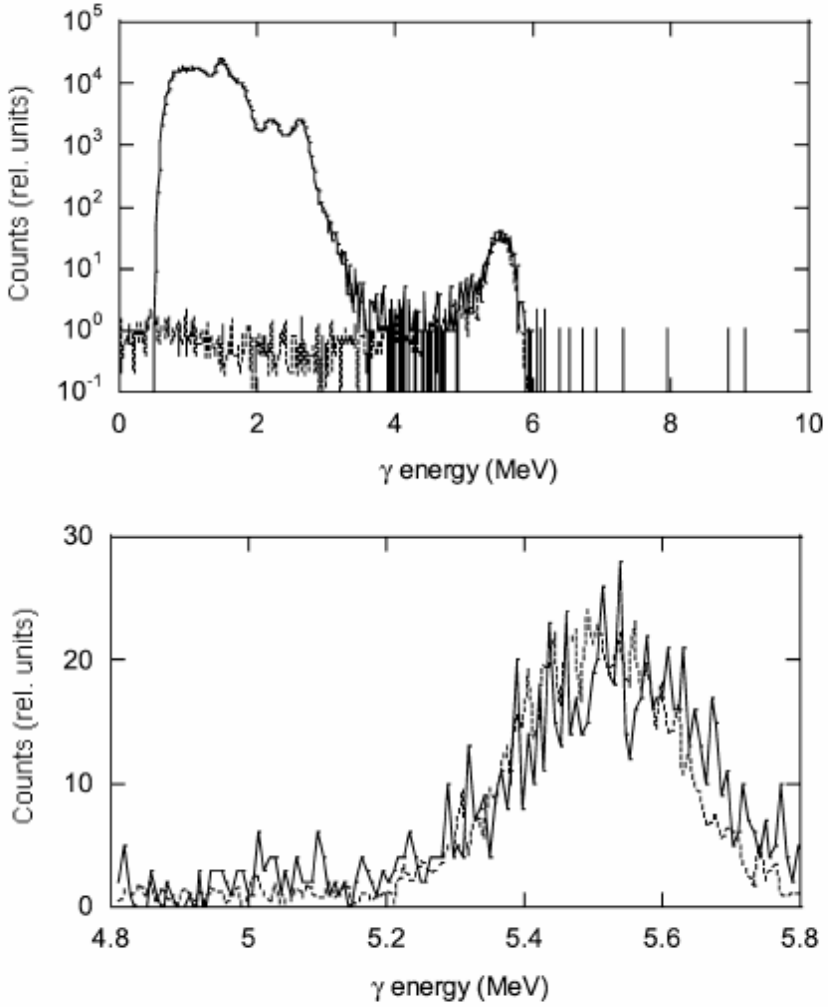

Fig. 2. Experimental (black line) and simulated (gray line) spectra of the 5.5 MeV photons from d(p, γ)^{3}He collected by the LUNA BGO detector for an interaction energy of 6.5 keV (center of the solar Gamow peak); nominal target pressure = 0.2 mbar. Spectra have been normalized to the maximum of d(p, γ)^{3}He peak. Top panel: full energy range; bottom panel: zoom of the region of interest for d(p, γ)^{3}He.

LUNA ^{3}He(α,γ)^{7}Be experiment: Phase I, detected ^{7}Be activity

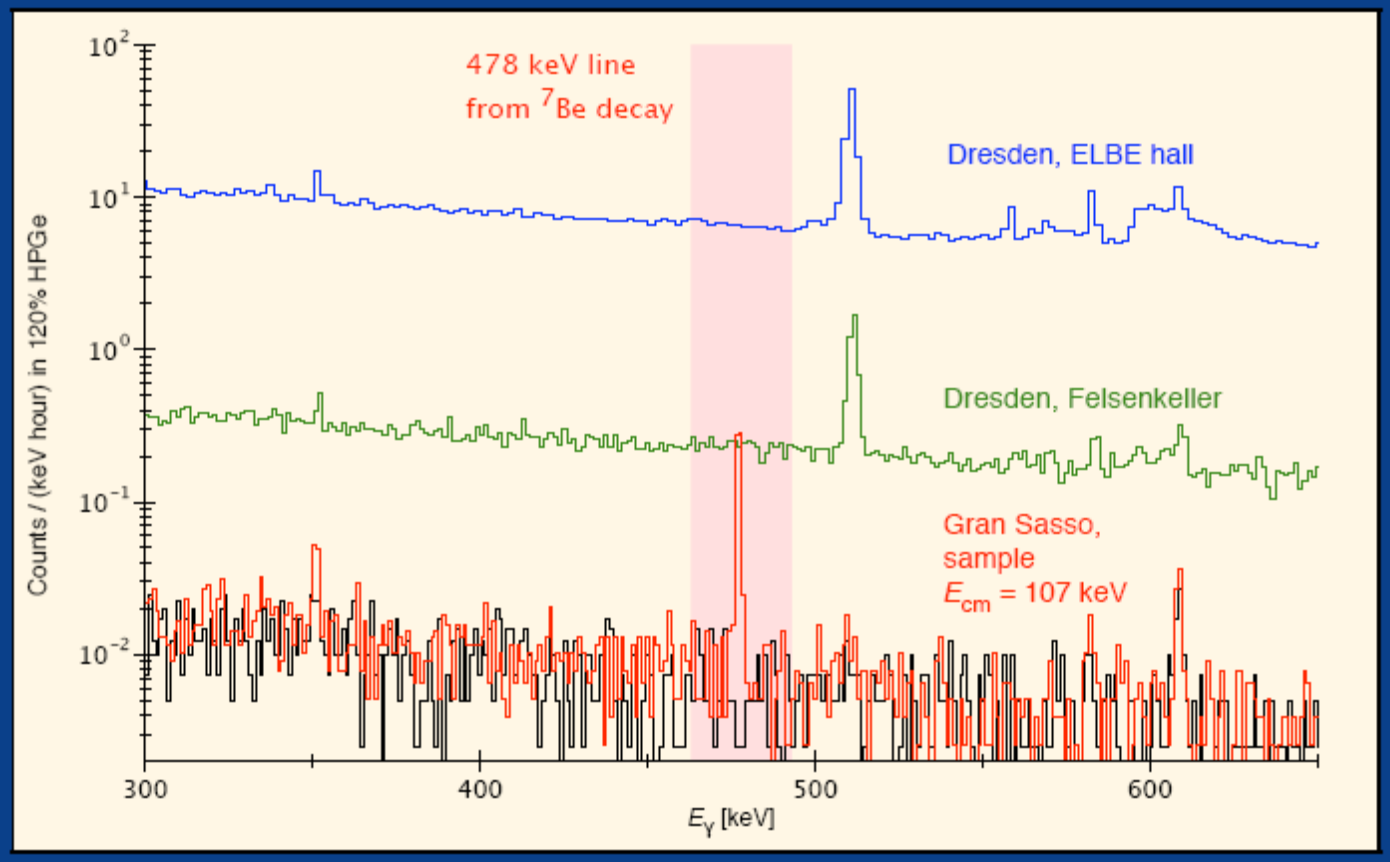

Activated ^{7}Be samples of 0.8 — 600 mBq

This example: 25 mBq

$^{14}N(p,\gamma)^{15}O$ LUNA 2002

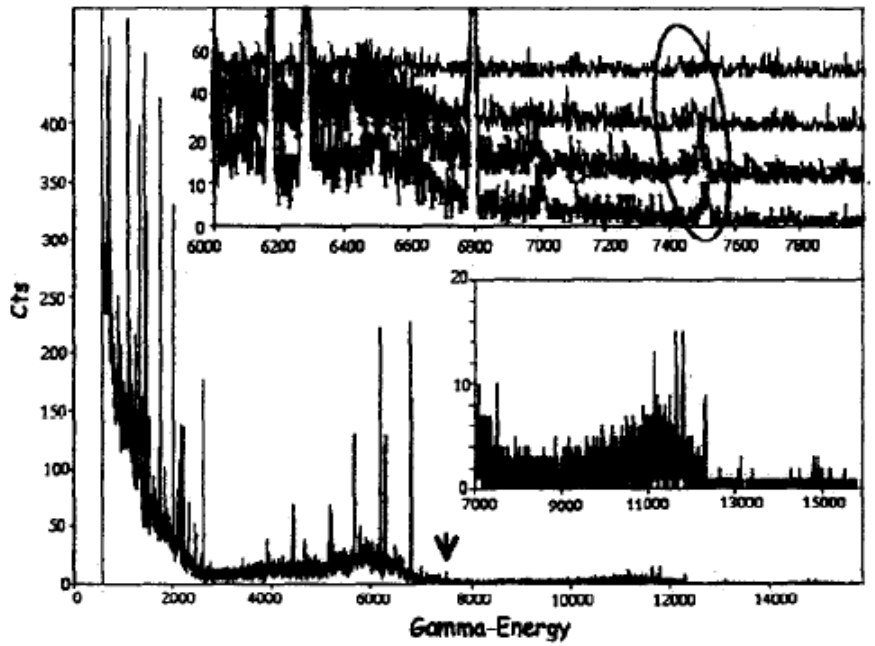

Figure 5. Typical spectrum of the reaction $^{14}N(p,\gamma)^{1)}O$ measured at a beam energy of 240keV. The arrow indicates the region of interest for direct ground state transition (R/DC→GS). The top insert shows the spectra measured at beam energies of 180, 200, 220 and 240 keV (top to bottom) in arbitrary units. The oval indicates the region of interest for the direct ground state transition. The bottom insert shows the high energy part of the spectrum dominated by the reaction $^{11}B(p,\gamma)^{12}C$.

$^{14}N(p,\gamma)^{15}O$ LUNA 2005

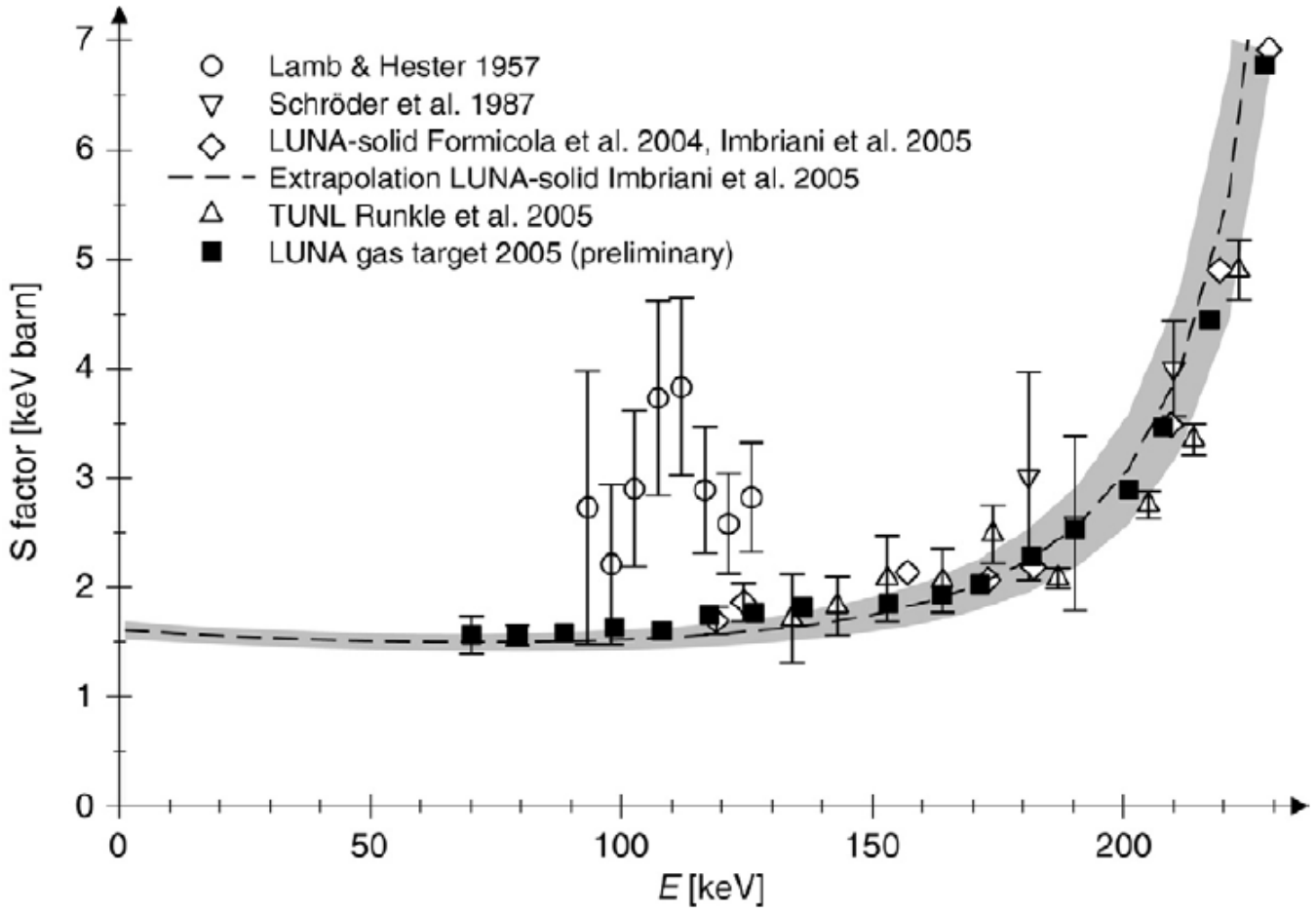

Fig. 4. Astrophysical $S(E)$-factor of ^{14}N(p, γ)^{15}O as a function of the center of mass energy E. The errors are statistical only.

$^{14}N(p,\gamma)^{15}O$ LUNA 2006

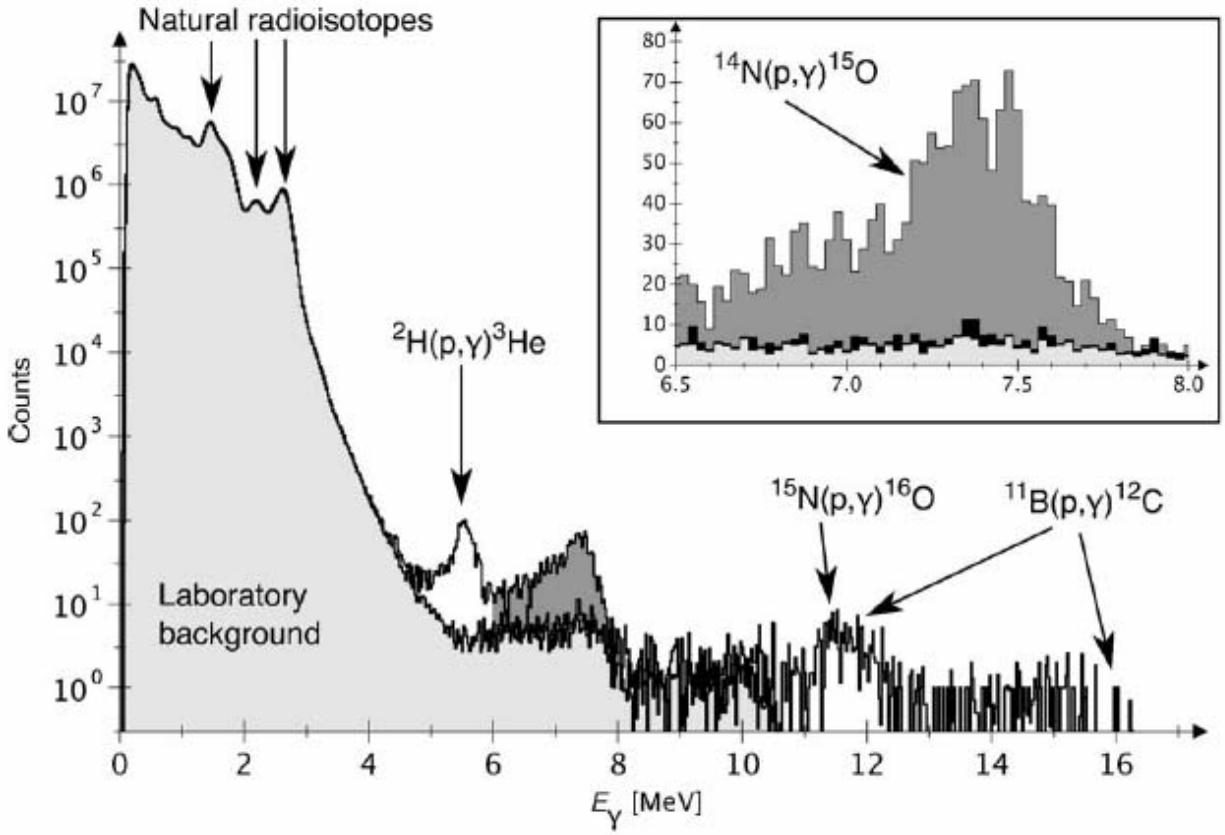

Fig. 1. Typical γ ray spectrum in the 4π BGO detector, at $E = 90$ keV, livetime 11.4 days, accumulated charge 231 C. The counts from the reaction to be studied are shaded in dark gray. The laboratory background [21], normalized to equal livetime, is shaded in light gray. The most important components of background induced by the ion beam are indicated. Inset: Region of interest (ROI) for the present study, with the beam induced background in the ROI indicated by the black filled area (see text).

$^{14}N(p,\gamma)^{15}O$ LUNA 2006

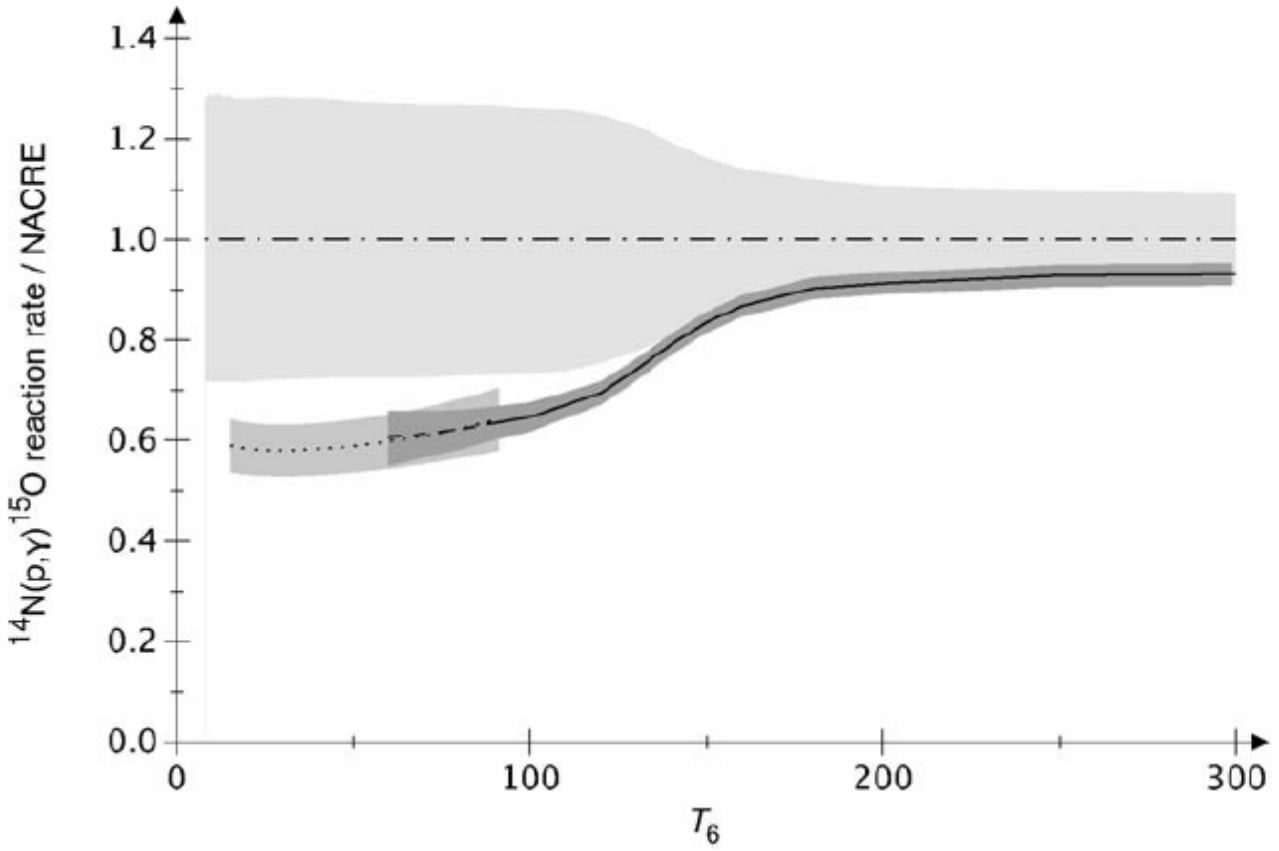

Fig. 3. Thermonuclear reaction rate relative to the NACRE [11] rate. Dot-dashed line: NACRE rate. Solid (dashed) line: present work and more than 90% (more than 50%) of the Gamow peak covered by experimental data. Dotted line: Extrapolation-based rate from Ref. [17]. The shaded areas indicate quoted upper and lower limit for the NACRE rate [11] and $\pm 1\sigma$ statistical uncertainty for the rate from Ref. [17] and the present work.

ERNA $^{12}C(\alpha,\gamma)^{16}O$ Q=7161.91 keV

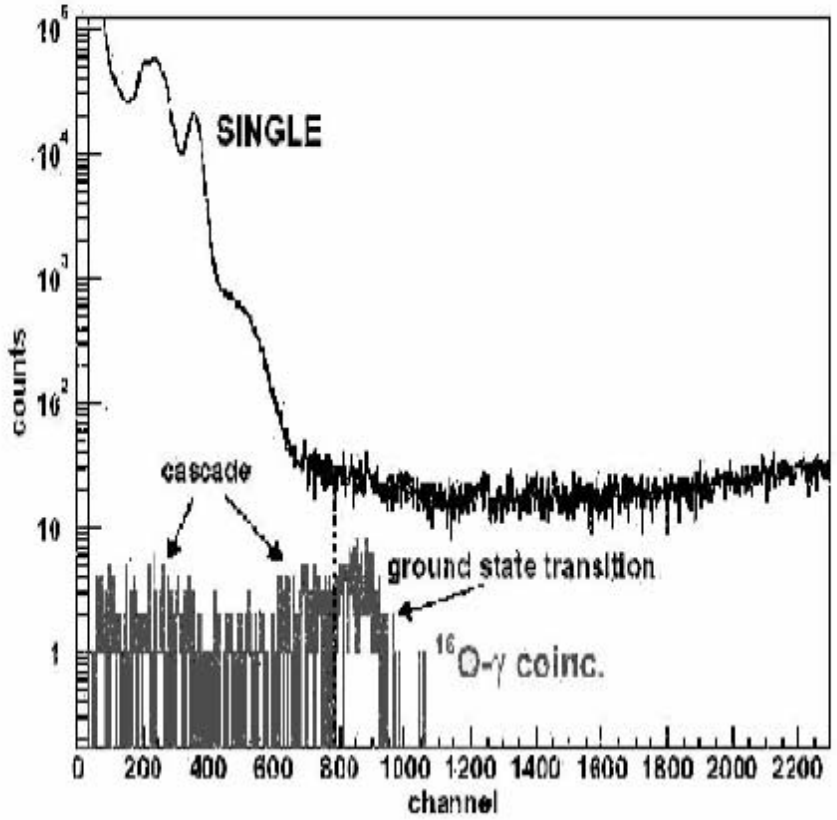

Figure 5. Background reduction in γ-ray spectra obtained in coincidence with the recoil

Layered shielding (reduce γ, β, neutrons)
Cu walls (cleanest material)
Thin "mu-metal" magnetic shield
Inner polyethylene (further neutron moderation)
Outside Pb & inner "ancient" Pb (low in ^{210}Pb)
Outer polyethylene (main neutron moderator)
All materials near detectors screened for U/Th/K

FUTURE

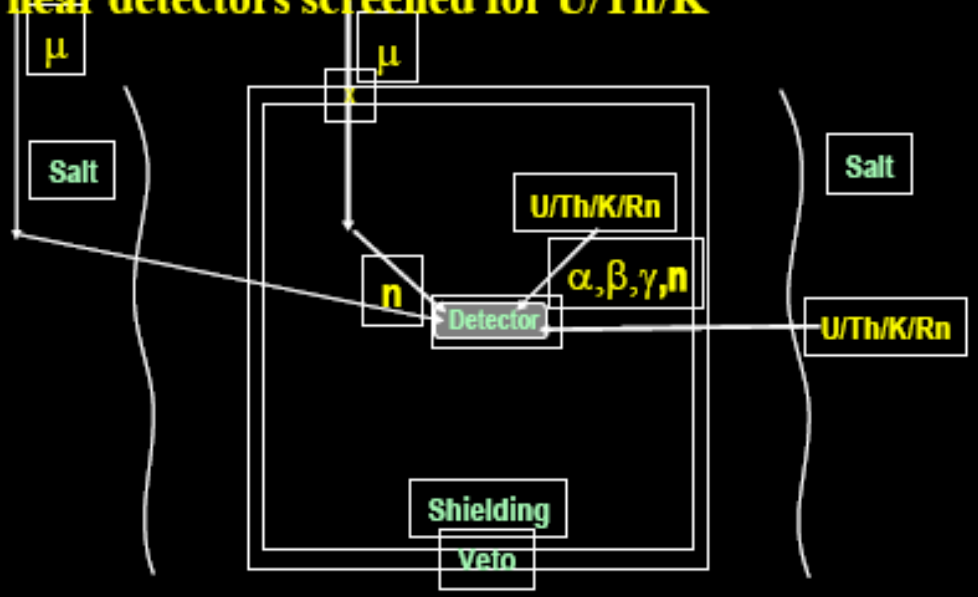

Active Veto (reject events associated with cosmics)
Thick plastic scintillator veto wrapped around shield
Reject residual cosmic-ray induced events

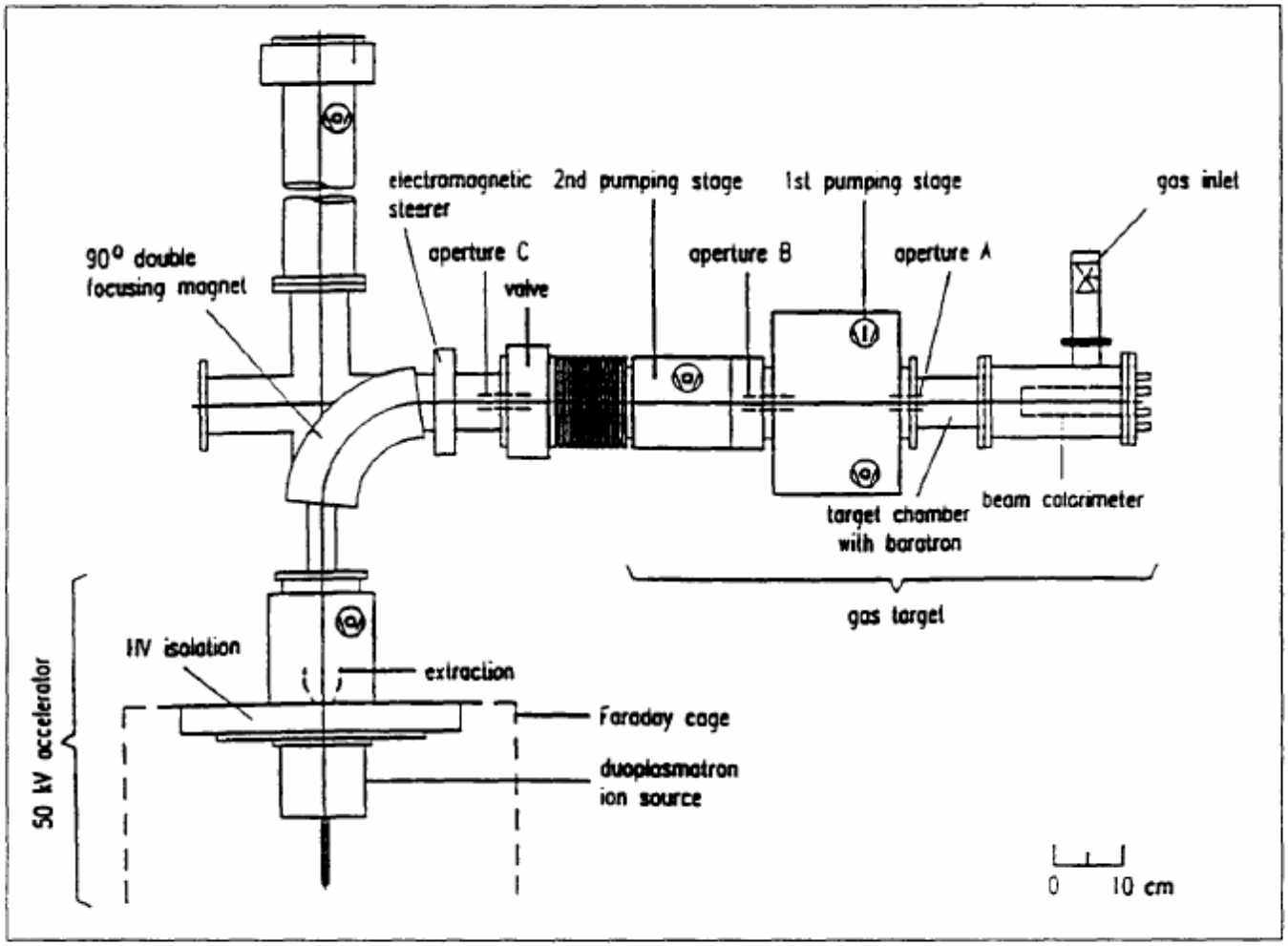

Figure 1. Schematic diagram of the 50 *KV* LUNA facility.

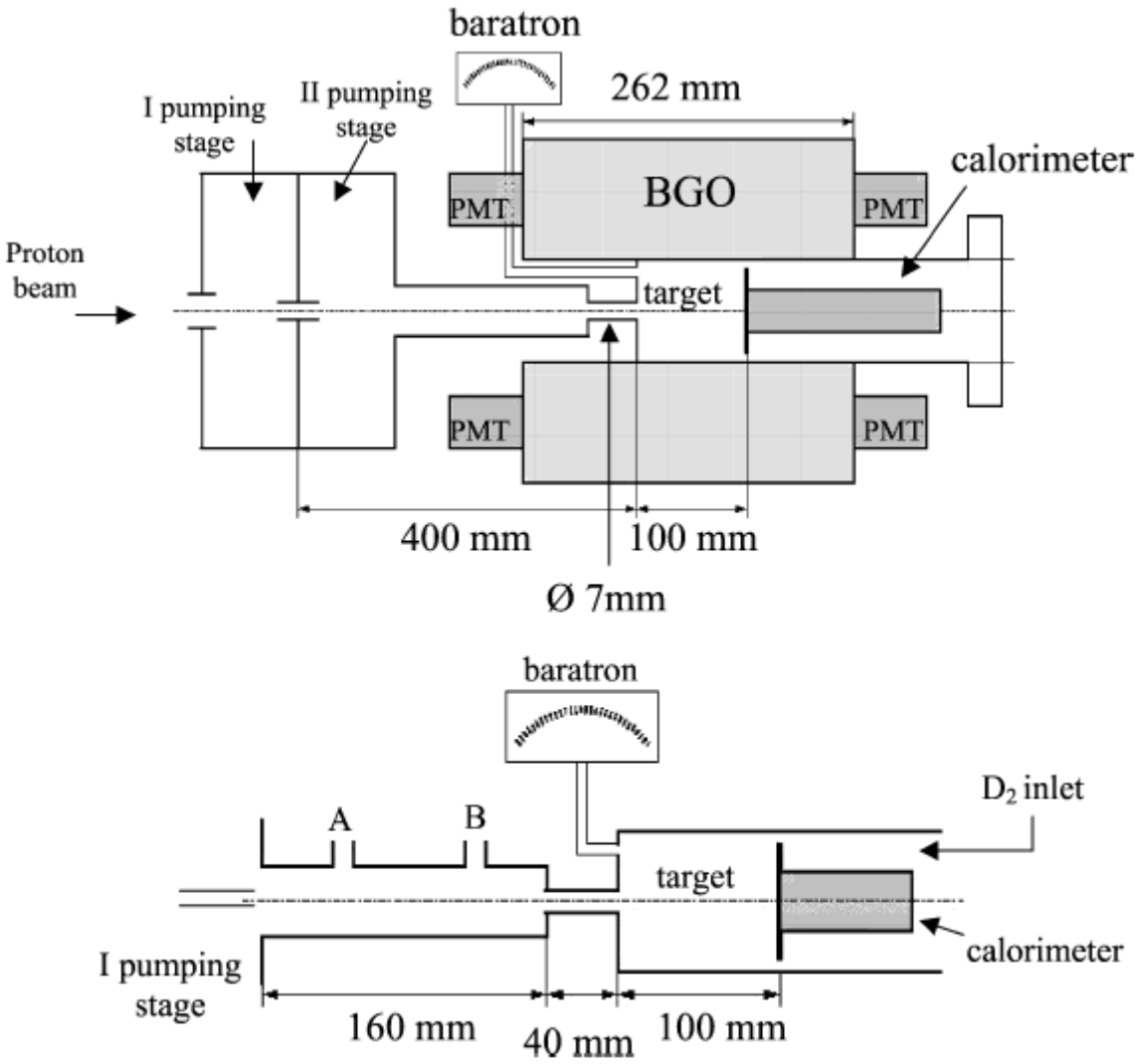

Fig. 1. Scheme of gas target set-up and BGO detector (top panel). In the bottom panel the geometry of the target zone and the points inside the first pumping stage, where the pressure profile was measured with an ad-hoc set-up with two apertures (labels A and B) are shown. Lengths in both panels are given in mm unit.

Detectors

Since **Germanium detectors** have been used for the measurement of the $^{12}C(\alpha, \gamma)^{16}O$ cross section, which provide a high **energy resolution** but **lack of efficiency**, **high beam currents** of up to 700 μA have been used in spite of possible target problems.

A different approach is the use of detectors with **high efficiency** such as **NaI** or **BGO**. Although in principle promising, these setups suffered from a **small solid angle** and relatively **high backgrounds**.

In contrast, the Karlsruhe **4π BaF_2** detector offers a **high gamma-ray efficiency** of up to 90% by covering 97% of the 4π solid angle and a comparably **low neutron sensitivity**. The detector is divided into 42 hexagonal and pentagonal segments. Each segment, except one for the beam entrance, holds an independent detector module consisting of a BaF_2 crystal with a thickness of 15 cm and a distance to the sample of 10 cm. All segments cover the same solid angle. This allows the simultaneous measurement at 12 different angles with respect to the beam axis, which is necessary since the E1 and E2 components need to be extracted from angular distributions to permit a reliable extrapolation to astrophysical energies.

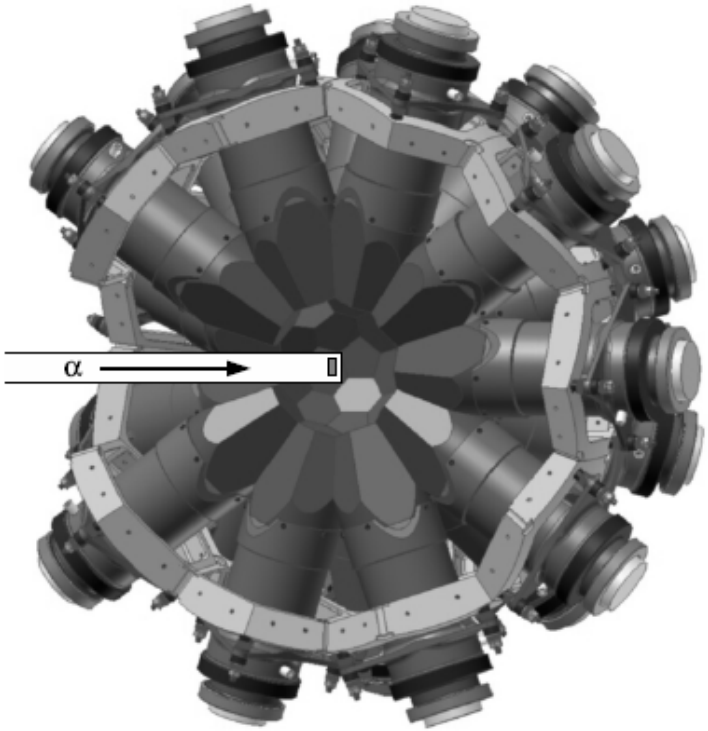

Figure 1. One of the two hemispheres of the Karlsruhe 4π BaF_2 detector.